INIS-mf--8981

CONTRIBUTIONS TO THE 12 th INTERNATIONAL CONFERENCE ON SOLID STATE NUCLEAR TRACK DETECTORS

ACAPULCO, MEXICO

September 4-10, 1983

INSTITUTE OF NUCLEAR RESEARCH
OF THE HUNGARIAN ACADEMY OF SCIENCES
DEBRECEN, HUNGARY

TABLE OF CONTENTS PREPRINT No.

ATOMKI Preprint E/2 (1983)

CURRENT PROBLEMS IN CHEMICAL TRACK ETCHING*

G. Somogyi

Institute of Nuclear Research of the Hungarian
Academy of Sciences, H-4001 Debrecen, Hungary

ABSTRACT

A schematic survey is given on the current relevant problems of the etching (or revelation) of multi-track and single-track events in dielectric solids. Some aspects of the research trends and possible new applications of the effects observable here, are also considered.

KEYWORDS

Nuclear tracks; radiation damage; chemical etching; etch-track kinetics; sensitivity curve; single- and multi-track effects.

INTRODUCTION

I have been asked to say a few introductory words on the chemical etching of nuclear tracks in solids. The hazard of such a task is obviously very large because this track revelation method has already been known for more than twenty years. At the same time it seems to be a very inspiring work since it appears certain that the potentialities of this method, in spite of its frequently emphasized simplicity, has not been fully realized. The truth of this statement had already become apparent at the previous track detector conference held in Bristol, and I am convinced that the latest experimental attacks by the great many researchers with a variety of new ideas are able to provide even more stricking advances in this apparently saturated field of researches.

The childhood of the chemical track etching technique is certainly over. A sure sympthom of it is expressed also by the fact that the first pioneers of this method are getting more and more respected, at least in consideration of their age. Fortunately, more and more young people have been working with this technique with new imaginations, dreams and enthusiasm. Some of them likes to follow old traditions, but there are also impressionists. In these circumstances there is no doubt that the statistical probability of finding something new in our field is enhanced.

Here immediately a further question arises: how wide would be the range of possible promising investigations where one could even refine, combine or perhaps discover "etching or related effects" which might be of theoretical or "only" practical importance? At the present conference, among others, a welcome opportunity is also provided for all of us to discuss this complex question, and to fill up our memories and recharge our batteries for future researches. My honourable duty here would be to promote shomewhat this procedure, at least in the field of track etching in polymers and in related problems.

New scientific developments are usually initiated and stimulated by well-established traditions and original ideas or by successful combinations of these approaches. Cooking recipes, certainly, cannot be delivered here for making progress. It is my hope, however, that I may help it a little by presenting certain characteristic directions and problems of the recent

* Invited paper.

researches concerning the track etching as a starting point of discussion.

RECENT RESEARCH TENDENCIES

One of the clearly noticeable advances has resulted from the systematic studies made by numerous track laboratories all over the world. These works have promoted to find promising new ways in both the basic research and application of nuclear track detectors. At the same time, as a usual consequence of the large number of studies, some of the already forgotten old methods and track revelation tricks were again find out, improved and applied in several laboratories.

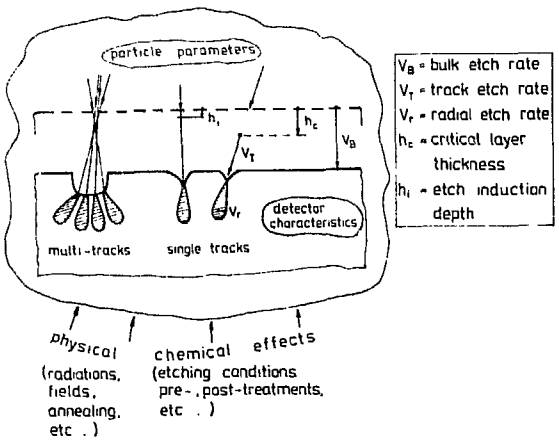

Fig.1. Schematic representation of recent objectives of studies in the field of track etching and related effects.

A schematic representation of the general fields of actual studies related to the chemical etching and related problems is given in Fig. 1. Information on the etching characteristics of a track detector under given conditions can be derived either from non-overlapping single tracks or from so-called multi-track effects. Till now, most of the research laboratories and track users has paid attention, almost exclusively, to the behaviour of single tracks. In addition, this behaviour has mostly been derived from the average properties of several single tracks. This procedure, of course, is appropriate in many practical works, by it, however, we cannot gain definite results concerning the etching response for an individual particle damage. In the latter case it is more adequate to study only one "track cone" in a thick sheet or one "track pore" in a thin foil.

The general behaviour and specific etching characteristics of both the single- and multi-track damages are governed and affected by several factors such as particle parameter, detector characteristics and environmental (physical, chemical and other) effects. All of these clearly indicate the wide variety and complexity of the possible research problems in this field. Let me select here, only to my taste, a few of them for discussion.

Research and Perspective of Multi-Track Effects

At first, I would talk on the multi-track effects, trying to outline certain new possibilities which arise from the following questions: What is to be done at very high track densities where the tracks begin to overlap? Can we find here any effects which may provide something new or useful, whether in basic science or in practical works, in addition to the more or less known single-track etching effects? Before answering these questions, I would say few introductory words of philosophical nature. As a starting point, let me remind you, what I had previously said, that an effective and creative researcher should be not only a good scientist, but also an impressionist with broad phantasy. Having this ability, one can imagine everything and then, by using special filtering process or transformation, even fantastic products of imagination can be turned into realistic, but in many cases into unexpected and surprising new results. It is my filling that the multi-track effects may give rise to such a new dimension of researches, and considering the pssible practical value of these effects, perhaps it is the time to learn the term "nuclear track technology", as proposed by Spohr and his coworkers, the pioneers of this field of researches (Sphor, 1981; Fischer and Sphor, 1982).

To illustrate the situation generally, let me mention an analogous example from the field of modern arts. Recently, a new possibility is opened for the development of a so-called "computer graphics technology" based on the

availability of fast and cheap computers. The idea is that the computer, by using appropriate geometric transformation and calculation rules, can turn the algebra into pleasing patterns in a variety of ways. The dropping and lifting pen of a plotter can draw thousands of lines with high speed and accuracy, creating surprisingly new images from great number of simple geometrical elements. Such a plane pattern of numerous tessalating hexagons and stars is shownin Fig.2, after an invention by Dixon (1983). Here, by using a simple geometric transformation called inversion, a new element, a sphere, is created.

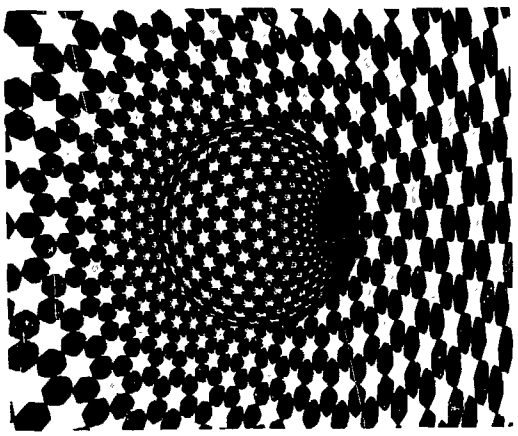

Fig. 2. A surprising new image element, a sphere, appears in a computer-made graphics specially constructed from numerous tessalating hexagons and stars (after Dixon, 1983).

Now, let us assume that in a given detector area we begin to increase the number of certain image-building elements (e.g. etch-pits of nuclear tracks) by using appropriate rules (e.g. specific irradiation geometry, energy distribution, etc). It is expected that over a given fluence, these elements get to overlap and form zones which display no similarity to the shape of original building elements. At this point, a new world is opened for us, with quite new microscopical and macroscopical, physical and chemical properties. I would like to illustrate this world somewhat, at least by few examples taking from our field of track researches.

When a sufficient overlap occurs between neighboring etched tracks, the resulting effect is the formation of a multi-etch-pit geometry with a labyrinth-like spatial texture. This texture developed at about 70 % porosity of the track array results in a very dramatic change in the electrical resistance of the exposed surface, as has pointed out by Fischer et al (1982). In this way, the resistance of surfaces can be increased by ten orders of magnitude. The abrupt appearance of this special effect due to multi-track etching, makes the preparation of superinsulating surfaces possible. It is interesting to note that this phenomenon disappears at higher track density, where the nominal porosity will be over 200 % and the surface texture develops again more fused and therefore more conducting etched cavity system. The inherent advantages and large perspectives of such type of multi-track etching effects are obvious if we take into account the wide range of available imaging elements and schemes. At present, we can use very well-defined ion ranges at arbitrary angles of incidences to generate very fine or rough, shallow or deep etch-track structures.

As a second example of the multi-track effects I have chosen the case of overlapping damage zones itself (i.e. high-fluence unetched tracks). Here, the overall effect of individual track damages transforms the overexposed detector area into a huge damage zone. In this zone, under ion bombardment, different physical and chemical processes occur, in polymers e.g. such as chain scission and crosslinking. The ion beam may also act as an "alloying agent". The modified surface then can be "developed" by different procedures, which are not necessarily etching processes. For example, an enhanced dissolution even by water (Somogyi et al., 1983) or a preferential dyeing (Loose et al., 1983) can also be successfully applied to make the overexposed regions visible. Such multi-track effects can be induced in a variety of materials, even in non-etch-track forming solids (e.g. in gelatine and hydrate cellulose) and by various type of particle beams with very short tracks (corresponding to about 1 keV/amu implantation energies) or very long ones (produced by relativistic heavy ions). Therefore, it is expected that an intensive research of these etching, dissolution and related effects may open new doors for many of future applications of the nuclear track method. Such a fruitful influence has already become evident in lithography, where tremendous interest has recently been generated by the ion-induced relief patterns developable in various polymeric resists (Adesida, 1983) or in quasi-photoresist materials (Sphor, 1981).

The study of selective etching and other processes in multi-track events may

result in new information on the microscopic nature of latent tracks also, in the region of very low and very high damage densities as well. This would give rise to a better understanding of the "radiation and etching response" of various detector materials to nuclear particles. A possible way of such attemps has been shown by Lück (1983a) who has tried to analyse the shape of response curves derived from experimental data available in the literature. From the analysis of the dose dependence of bulk etch rates in gamma- and electron-irradiated CN, CR-39, PC and PET sheets, it has turned out that the relation describing the bulk etch response can be composed of a linear and a supralinear (power) term, while the linear term is absent from the response curve related to single nuclear track etching. The only expection seems to be the CR-39 detector. According to Lück (1983) the appearance of supralinear term can be understood by a model of free reaction volume, which assumes that the etchant requires a given free volume of hole, produced by release of gaseous radiolysis products, to be able to attack the chemical chain successfully.

Finally I choose my last example from among the problems of conventional autoradiography using nuclear track detectors. Here, the quality of image is affected considerably by the presence of multi-etch-pit configurations. We should encounter, however, the following paradoxial situation: High resolution autoradiography can be made only by using high-density picture-forming elements to reduce the image unsharpness due to the statistical spatial fluctuations of the number of elements. At the same time, however, the etch pits begin to overlap and produce a continually decreasing optical contrast, which decreases the quality of image. This etching effect was already studied as early as 1971 (Somogyi and Srivastava, 1971) but, due to it complexity, the image formation under this special condition, was treated theoretically only recently (Ilić et al., 1982).

By these arbitrarily selected examples I wanted to demonstrate the importance of having more information on the effects created by multi-track events and on their inherent perspective in many useful applications. As concerns other interesting phenomena generated by microcavities embedded into various solids by track etching methods, I refer only to a very recent comprehensive survey by Fischer and Sphor (1982).

Research of Single-Track Behaviour

Now, I come back again to the illustration shown in Fig. 1, where I have drawn a rough sketch of the general objectives of actual researches of single-track behaviour. Here, of course, I have no opportunity to consider all of the relevant interesting research directions and problems, My only alternative should be again some kind of selection, which is necessarily subjective.

At first, I would mention some problems concerning those parameters which govern the track-etch kinetics. At present, to describe the main aspects of etch-pit evolution, the following basic quantities are enough to be taken into consideration: the bulk etch rate (V_B), track etch rate V_T , radial etch rate (V_r), critical layer thickness (h_c) and etch-induction depth (h_i).

I think, there are authors who would like to see on my list also the so-called "detection or registration threshold" expresed in terms of critical particle range (R_c), energy (E_c) or some kind of energy loss (e.g. REL_c) or dose density. In most of the cases, however, due to a steady, slow approach of the etch rate ratio ($V = V_T/V_B$) to one, toward longer residual particle ranges (R), such a detection threshold cannot be extrapolated, or if at all, only with very small precision. Therefore, this parameter is not suitable for fine quantitative description, and in addition there is no need for it in any analysis of the condition of track appearance. Accordingly, I have omitted it from my list. Perhaps it may serve as a classification guide for an approcimate comprison of the relative sensitivities of various detector materials. But, even for this case, it is more reasonable to define a so-called "practical detection threshold" at a low, but well-measurable etch-rate ratio, say at 1.2 (and not at 1 !). For this, of course, a careful measurement of the variation of etch-rate ratio along the hardly etchable portions of particle trajectory is required. From this consideration it is obvious that the so-called sensitivity curve, defined by the V(R) function, is a more fundamental quantity than the detection threshold derived from it.

Having omitted the detection threshold from our list, we might belive that

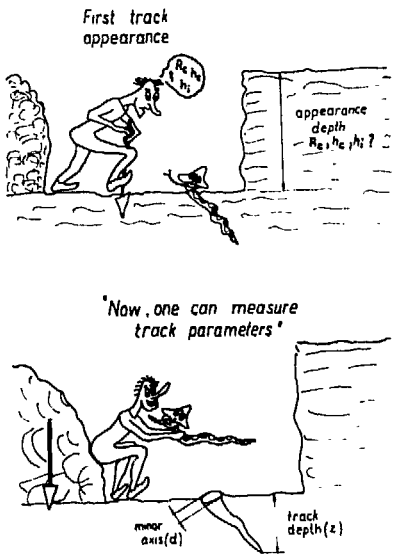

Fig. 3. Drawing illustrating an important behaviour of track method: the abrupt appearance of certain etch-pits at a given depth below the original surface.

the situation has become more clear. But it is only partially true, because there exist even two other quantities, h_c and h_i, which also describe threshold-like phenomena in the etch-pit appearance. Knowing this situation we may understand the serious problem of the newcomers in our field, or sometimes even the more experienced research workers, when they find a threshold-like track appearance in their detectors (see Fig. 3). They should ask themself which quantity should be actually applied to describe the observation: R_c, h_c, h_i or perhaps certain combination of these? Fortunately, the critical layer thickness, can also be derived from the sensitivity curve of a particle.

Before discussing the nature of h_c and h_i, we have to deal a little with the sensitivity curve which is the base of any calculations related to the track evolution during chemical etching. Although there have been several efforts to find the link between the parameters of radiation damage and chemical ethcing, even at present, the determination of the shape of sensitivity curve is an empirical task. Researches in this field are disturbed by the fact that the parameter (V) describing the registration sensitivity is a complicate function of the particle parameters, material effects and etching conditions. Recently attemps have been made by several laboratories to elucidate somewhat the situation here (e.g. O'Sullivan et al, 1982; Green et al, 1982; Lück, 1983b and 1983c). From 28 individual response curves, Lück (1983c) has succeeded in deriving a more general form of the response function, V(REL). (We note that from this function V(R) for a given particle can be easily obtained.) He has found that for pure cellulose nitrate detectors, prepared with different degree of substitution, the usual $V = 1 + \alpha \cdot REL^{\beta}$ form of the response function can be formulated only with one fitting parameter, since α and β are connected to each other by the relation of $\alpha = 8.12 \times 0.011^{\beta}$, independently on the detector and etching parameters used. In addition, it has been found that V_B appears to be associated with the fractional amount (F) of disubstituted CN by the relation $V_B = 1.15\ (1 - F) + 48.9\ F^2$ (Lück, 1983b).

In spite of achieving certain successes in the above mentioned field, the profundity of our knowledge is far from satisfactory. Further researches are still greatly needed to learn more about the factors influencing the etching response in various detectors to different, low and high energy nuclei. Immediately after discovering its unique sensitivity (Cartwright et al, 1978), the CR-39 polymer appeared to be the best test material in this respect, because the shape of etched tracks displayed nearly perfect geometry in it. Since that time, however, according to relevant studies (see e.g. Somogyi, 1982 and its Reference list; Green et al, 1982), here also many "side-effects" have been reported (depth dependent response, "ballooning" of tracks, etc), which have made more difficult to draw general conclusions. An additional disturbing effect is brought about the severe variations in the response of CR-39 products of different origin (see Fig.4) and even batches. Consequently, a sensitivity curve measured in a given laboratory usually cannot be directly applied in another laboratory, e.g. for calculation of etch-pit appearance and evolution.

There is also a lack of knowledge in the sensitivity curve at relatively short particle ranges. In this region, unfortunately, the function forms usually applicable at higher residual ranges give very different results. For sake of illustration, such function forms are plotted in Fig. 5. These curves can be used equally well for describing the sensitivity curves for higher energy protons in a Hungarian CR-39 products. In low energy region, however, without experimental etch-rate data, we could not select the adequate form of function.

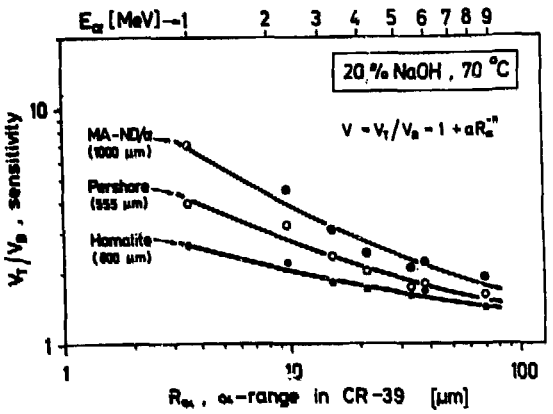

Fig. 4. Sensitivity curves of different CR-39 products for alpha-particles. The solid lines show the curves fitted by the indicated equation.

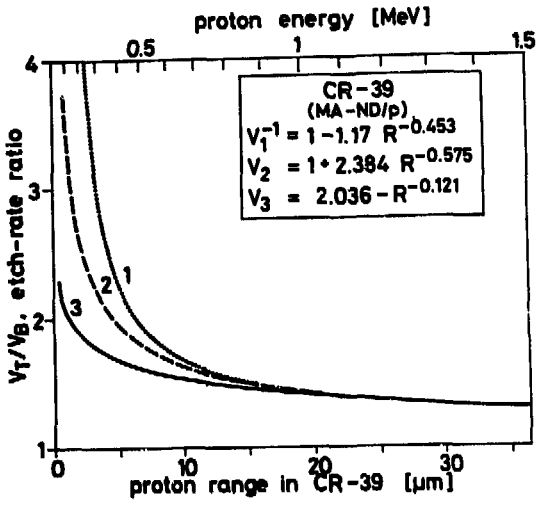

Fig. 5. Possible sensitivity curves of a Hungarian CR-39 product for protons. All the curves were fitted to the same experimental data above 1 MeV with a correlation coefficient $r \geq 0.98$.

A somewhat more sophisticated function for describing the sensitivity curve for alpha-particles in a wider range interval, including also the "peak region" of Bragg curve, has been proposed recently by Green et al (1982).

Having chosen the proper form of V(R) function, we can calculate the expected variation of track appearance depth determined by the quantity h_c. I note here that h_c actually was introduced by the author for varying etch rate ratio to replace the concept of critical angle (θ_c) of track registration, where θ_c becomes meaningless. The calculated curves shown in Figs. 6 and 7 well illustrate the complicated effect of this threshold-like phenomenon on the etch-pit appearances when using different irradiation parameters (incident angle, particle range) and CR-39 sensitivities.

The value of h_c, in principle, should be zero at right angle of particle incidence. This supply a possibility for us to separate the two effects described by h_c and h_i. The existance of etch-induction depth should be the consequence of a surface phenomenon, because no etch-induction time ($t_i = h_i/V_B$) can be observed in a pre-etched detector. It should also be noted that t_i is an inverse function of V_B for a given particle energy and it seems to be dependent on the radiation damage density. At present, the mechanism of the process responsible for the etch-induction period is not clear.

Here a few words should also be devoted to the radial etch rate denoted by V_r. This quantity can be considered as a transition etch rate between V_T and V_B, if we try to describe the variation of local etching speed at right angle to the axis of latent track around the track core. A continuous decrease of the etch rate away from the track core is already expected from the delta-ray model, according to which the radiaton damage is not limited only to a narrow cylindrical region of about 10 nm radius, but may extend to larger distances as well. For a long time, however, nobody has paid attention to systematic study of this radial track etching behaviour. Only recently, the production (or demand) of commercial nuclear filters by accelerated heavy-ion beams in various laboratories, such as Dubna (USSR), Darmstadt (GFR), GANIL (France), has raised more serious interest among physicists to try to study and describe the formation of submicron track pores of well-controlled geometry in thin foils (Apel and Pretzsch, 1983; Fischer and Sphor, 1982; Guillot and Rondalez, 1981). At the same time, efforts have also been made to correlate calculated damage density distributions around track core to etch rate data (Ditlov, 1980 and personal communication; Zamani and Charalambous, 1981; Apel and Pretsch,

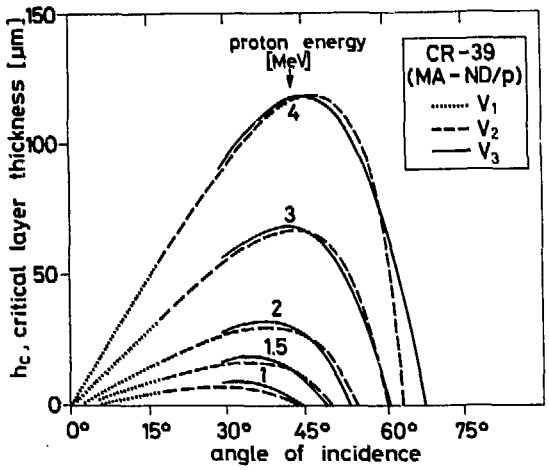

Fig. 6. Calculated curves showing the variation of the depth of track appearance with angle for protons. For calculation, the sensitivity curves shown in Fig. 4 are used. The curves denoted by V_1 and V_2 are identical above 16°.

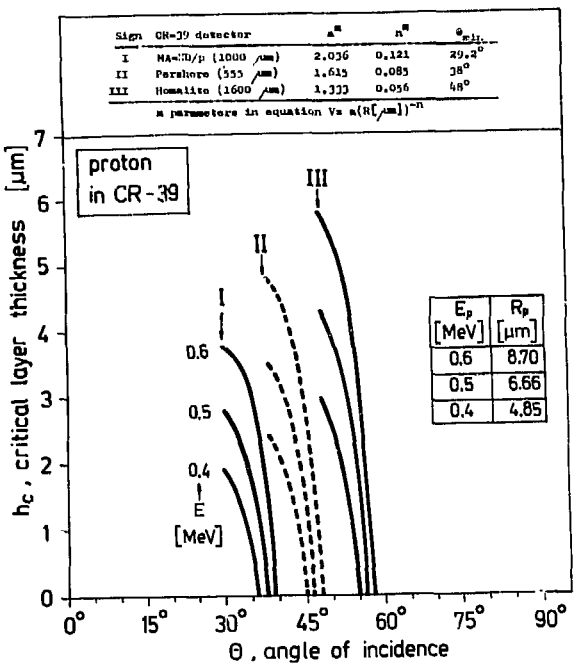

Fig. 7. Calculated curves showing the variation of the depth of track appearance with angle for protons in different CR-39 products. For calculation, the sensitivity functions given in the table above the figure are used.

1983). Such type of investigations may contribate considerable to a better understanding of the basic mechanism of preferential chemical etching both along the track and in radial direction to the track core. Experimentally, both the track and radial etch rate can be well determined with high precision, by using a conductometric measurement method for successive etching stages of the track pores, as was initially suggested by Bean et al (1970) and applied by DeSorbo (1979) for fission track studies in thin foils.

Finally, I should like to mention here a very exciting field of recent and future researches, namely the penetrability of damage zone (and also the bulk material) with etchant or other solutions. Unfortunately, only few data have been reported on these and related problems. At present even the mechanism of the first stage of etching process is not known, when the etchant ions begin to penetrate into the track core and the bulk material. The process should obviously be governed by the thermal diffusion of ions, characteristics of chemical reaction, and removal of reaction products. The overall rate-determining process, however, can be quite different in the bulk material and the damage region under different track revealing conditions (temperature, concentration). Taking into consideration only the diffusion, a two-phase track developing model is recently proposed by Törber et al., (1982) and a connected two-step soaking procedure for improving track revelation is described by Malinowski et al, (1982).

In the dyed-track technique, a great improvement in the efficiency of track revelation has also been reported by the use of a swelling process prior to the track dyeing. Such a pretreatment enhances the preferential penetration of dye molecules into the track core (Somogyi et al, 1979; Lferde et al, 1982). Very recently, based on an analogous idea in etching technique, a new identification method is proposed by Todorović, and Antanasijević, (1983). In their method an ultrasonically accelerated water penetration in the track, applied between two etching periods, has resulted in an increased chemical reactivity.

CLOSING WORDS

At the end of my talk, I would like to illustrate the present stage of the complexity of track business and research activity by means of a caricature. At the 10th International Conference held on SSNTDs in Lyon, I had already shown a sketch of a possible family tree of the nuclear track technique. To illustrate the situation at that time, I presented a more or less lonesome imaginary tree, in style of modern painters, with leaves loaded with many, different sort of fruits. These represented the very different type of possible products of the application of etch-track method.

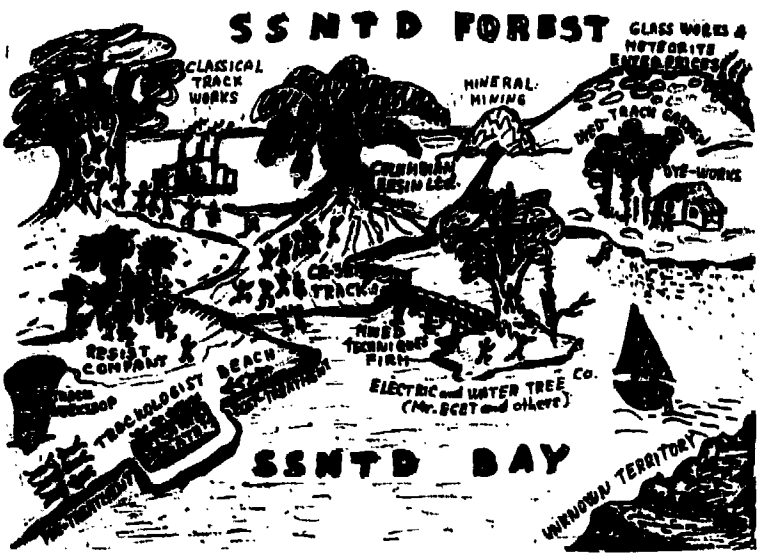

Fig. 8. A survey of the recent relevant fields of the SSNTD business and research activity.

At the 11th International Conference on SSNTDs in Bristol, I could already show a new repidly growing branch on the family tree, representing the birth of CR-39 track detectors. Since that time, the situation has become even much more complex as certain blossoming branches have begun individual life. In this way for the present time, as I have illustrated in Fig. 8, a SSNTD forest has come into life with a variety of research, business, management and other activities around it. These activities, of course, will need more and more land and bay and finally an establishment of Track Detector Society. Therefore, we should be very grateful to our Mexican colleagues that they have reserved this picturesque place in Acapulco, for trying to establish this Society, this place that will draw us back again and again to see the new changes in our ever-growing track forest.

REFERENCES

Adesida, I. (1983). Ion bombardment of resists, Nucl. Instrum. Meth. 209/210, 79-86.

Apel, P. Yu., and G. Pretzsch (1983). Investigation of the radial pore etching rate in a plastic track detector as a function of the local damage density around the ion path. Nucl. Tracks. to be published.

Bean, C. P., M. V. Doyle, and G. Entine (1970). Etching of submicron pores in irradiated mica. J. Appl. Phys. 41, 1454-1459.

DeSorbo, W. (1979). Ultraviolet effects and aging effects on etching characteristics of fission tracks in polycarbonate film. Nucl. Tracks. 3, 13-32.

Dixon, R. (1983).Geometry comes up to date. New Scientist, 5 May, 302-305.

Cartwright, B. G., E. K. Shirk, and P. B. Price (1978). CR-39: a nuclear track polymer of unique sensitivity and resolution. Nucl. Instrum. Meth. 153, 457-460.

Ditlov, V. A., (1980). Theory of spatial calculation of primary action of δ-electrons in track detectors with account of multiple scattering, Proc. 10th Int. Conf. Solid State Nuclear Track Detectors, Lyon, 131-141.

Fischer, B. E., D. Albrecht, and R. Spohr (1982). Preparation of superinsulating surfaces by nuclear track technique. Rad. Effects. 65, 143-144.

Fischer, B. E., and R. Spohr (1982). Production of nuclear tracks in solids and their use as a microtool. GSI-Report. (preliminary version), Darmstadt, July

8th 1982, pp. 71-103.
Green, P. F., A. G. Ramli, S. A. R. Al-Najjar, F. Abu-Jarad, and S. A. Durrani (1982). A study of bulk-etch rates and track-etch rates in CR-39. Nucl. Instrum. Meth. 203, 551-559.
Guillot, G., and F. Rondelez (1981). Characteristics of submicron pores obtained by chemical etching of nuclear tracks in polycarbonate films. J. Appl. Phys. 52, 7155-7164.
Ilić, R., M. Najžer, A. Podgornik, and M. Humar (1982). Radiographic characteristics of CR-39 detector. Proc. 11th Int. Conf. Solid State Nuclear Track Detectors, Bristol, Pergamon Press, 183-187.
Lferde, M., J-L. Seidel, M. Monnin, G. Somogyi, and M. Tóth-Szilágyi (1982). Diffusion processes in dyed detectors. Proc. 11th. Int. Conf. Solid State Nuclear Track Detectors, Bristol, Pergamon Press, 299-306.
Loose, A., I. Hunyadi, G. Somogyi, Zs. Varga, M. Najzer, and R. Ilic (1983). Neutron-induced autoradiography based on relief and dyed image formation in polymers. Proc. 12th Int. Conf. Solid State Nuclear Track Detectors, Acapulco, see present issue.
Lück, H. B. (1983). Bulk response of some polymeric nuclear track detectors to ionizing radiation, Nucl. Instrum. Meth. 212, 371-373.
Lück, H. B. (1983b). On the use of cellulose nitrate as solid state nuclear track detector, Part I: Detector preparation and etching behaviour. Nucl. Instrum. Meth. 212, 479-482.
Lück, H. B.(1983c). On the use of cellulose nitrate as solid state nuclear track detector, Part II: Response to light particles and applications, Nucl. Instrum. Meth. 212, 483-487.
Malinowski, I., W. Enge, G. Sermund, R. Beaujean, and G. Siegmond (1982). The diffusion-etch-model, Part II: First application for quasi-relativistic Fe-ion registration in Daicel cellulose nitrate. Proc. 11th Int. Conf. Solid State Nuclear Track Detectors, Bristol, Pergamon Press, 311-314.
O'Sullivan, D., P. B. Price, K. Kinoshita, C. G. Willson (1982). Proc. 11th Int. Conf. Solid State Nuclear Track Detectors, Bristol, 81-84.
Somogyi, G., and D. S. Srivastava (1971). Alpha radigraphy with plastic track detectors, Int. J.Appl. Rad. Isotopes, 22, 289-299.
Somogyi, G., M. Tóth-Szilágyi, M. Monnin, and J. Gourcy (1979). Non-etching nuclear track visualization in polymers: fluorescent and dyed tracks. Nucl. Tracks., 3, 151-167.
Somogyi, G., (1982) Status of development in the field of CR-39 track detectors. Proc. 11th Int. Conf. Solid State Nuclear Track Detectors, Bristol, 101-113.
Somogyi, G., I. Hunyadi, R. Ilić, A. Loose, and Zs. Varga (1983). Formation of ion-beam images in gelatine and various polymers. Proc. 12th Int. Conf. Solid State Nuclear Track Detectors, Acapulco, see present issue.
Sphor, R. (1981). Heavy ion nuclear tracks— an emerging technology, IEEE Trans. on Nucl. Sci. NS-28, 1448-1451.
Todorović, Z., and R. Antanasijević (1983). A new method for identification of low energy fragments with $8<Z\leq18$ in plastic track detector Makrofol. Nucl. Instrum. Meth. 212, 217-219.
Törber, G., W. Enge, R. Beaujean, G. Siegmon (1982). The diffusion-etch-model, Part I: Proposal of a new two-phase track developing model. Proc. 11th Int. Conf. Solid State Nuclear Track Detectors, Bristol, Pergamon Press, 307-310.
Zamani, M., and S. Charalambous (1981). Registration probability of alphas in cellulose nitrate. Nucl. Tracks. 4, 177-185.

ATOMKI Preprint E/3 (1983)

DEVELOPMENT OF THE DYED-TRACK METHOD FOR KODAK CN-85 DETECTOR

G. Somogyi[*], M.Tóth-Szilágyi[*], Zs. Varga[*], M. Monnin[**] and M. Lferde[**]

[*]Institute of Nuclear Research of the Hungarian Academy of Sciences, H-4001 Debrecen, Hungary
[**]Laboratoire de Physique Corpusculaire CNRS, IN2P3, Université de Clermont II, B.P. 45, 63170 Aubiére, France

ABSTRACT

The dyed-track method has been successfully developed for cellulose derivatives. The track parameters (width, coloration deepness, contrast, registration sensitivity), however, proved to be very dependent on the detector material and on the track processing conditions. In our previous works optimum conditions were presented mostly for cellulose acetate sheets. In the present work we have studied the influence of track processing parameters on the dyed-track formation in Kodak cellulose nitrate detector called CN-85. It is found that in this material optimum dyed-tracks can be produced with using no swelling but with a thermal annealing at 100 °C for 1 hour after particles irradiation. For sensitization a treatment with 15% HCl at 22°C for 20 hours and for dyeing 0.3 wt% Rhodamine-B at 100°C for 1 hour proved to be the best. For better understanding the track dyeing phenomenon we have studied the colouration behaviour of electron-irradiated CN-85 detectors.

KEYWORDS

CN-85 detector; dyed fission tracks; non-etching; sensitization; annealing; electron irradiation; colouration of cellulose nitrate.

INTRODUCTION

The first successful attempt to make latent fission tracks visible with a non-etching dyeing method was reported by Monnin and Blanford (1973). Primarily, it was assumed that a narrow, active region (containing metastable chemical species such as free radicals, peroxide, etc) is created along a particle path in a polymer, therefore by using an unsaturated acidic monomer new polymer chains can be grafted onto the species of active region. Then, a fluorescent basic dye, Rhodamine B, can be built up onto the supposedly formed polyacid graft-copolymer and the tracks can be made visible under UV-light illumination.

It was soon discovered by Somogyi (1976) that a graft-copolymerization mechanism could not be responsible for the observed dye-track formation because tracks can also be revealed with using saturated acidic monomers. This finding justified the use of another term than "grafting" for the acidic treatment, namely the term "sensitization". It was also shown that by applying a treatment with a swellant (e.g. NaOH) to certain cellulose derivatives (especially to cellulose acetate) the width of dyed fission tracks can be increased so greatly that the tracks could be seen even under normal visible light illumination.

In other works (Somogyi and Tóth-Szilágyi, 1977; Somogyi et al, 1979b) it was pointed out that an additional improvement of the dyed-track technique could be achieved by using inorganic acids of low pH value as "sensitizing agent".

Finally, a procedure consisting of three main steps: basic swelling, inorganic acidic sensitization and dyeing with Rhodamine B, was introduced as a standard method of efficient dyed track revealing (Somogyi et al, 1979a and 1979b;

Mommin et al, 1979). In a systematic research we have found the proper concentration, temperature and time of treatment for each steps in cellulose acetate and we could get optimum, well-contrasted dyed tracks for fission fragments and even for neutron-induced recoils. We have been, however, much less successful at dyeing nuclear tracks in cellulose nitrate sheets (Somogyi et al, 1979b) when using the same track processing parameters which proved to be optimum for cellulose acetate. For cellulose nitrate we could get dyed tracks with sufficiently high registration efficienty only under UV-light illumination

Therefore, we have started systematic studies to get a better understanding of the track formation mechanism in this type of detectors, particularly the diffusion ability of the reagents used in the three track revealing steps (Mommin et al, 1979; Lferde et al, 1982) and the effect of thermal annealing on the dyed track formation (Mommin et al, 1980).

From these studies we have got evidences that the swelling agent diffuses only partially through the bulk of detector, on the contrary, the acidic molecules diffuse within the whole of polymer with a rather high speed and the dye molecules penetrate preferentially along the latent tracks and then only very slowly sideways. Considering this, the key of a further improvement of the dyeability of tracks in cellulose nitrate film seemed to be an enhancement of the condition of dye diffusion. It was assumed that the introduction of a thermal treatment after particle irradiation might induce a more penetrable structure of the bulk material and, in addition, a more advantageous lateral diffusion of the dyeable active species. In the present work the latest results achieved along these lines will be summarized. Furthermore, an effort for simulation of the behaviours of dyed track formation by studying the colouration intensity of electron-irradiated CN-85 sheets will be presented.

EXPERIMENTAL CONDITIONS

For all of our present studies the detector samples were chosen from the same batch of 100 μm thick CN-85 sheet (Kodak-Pathé product).

For the dyeing experiments described herein, given areas of the samples were irradiated by fission fragments provided by a Cf-252 source in 2π-geometry or by 450 keV electron beams accelerated by the Cockroft-Walton generator of the Institute of Nuclear Research in Debrecen (Hungary).

In each set of experiments first the irradiations were carried out, then the CN-85 samples were hanged up in an oven and submitted to thermal annealing. The annealing was followed by a sensitization procedure by immersing the sample into water solution of an inorganic acid (usually 15% HCl at 22°C). After sensitization the samples were dyed in a water solution of Rhodamine-B (in the following Rh-B), usually at boiling temperature for 1 hour. After each above-mentioned procedure an additional washing step was also applied in water at 70°C for 0.5 hour. We note here that the track revealing parameters actually used will be given in each cases in the respective figures under the following abbreviations: An (=annealing), S (=sensitization) and D (=dyeing).

The dyed fission tracks were finally viewed and counted under an optical microscope at 500 X to determine the registration efficiency as compared to that of the chemically etched tracks. For the track width determinations a magnification of 1000 X was used. The optical density measurements of dyed electron-irradiated samples were performed by a Zeiss microphotodensitometer.

RESULTS AND DISCUSSION

In one of our first studies we have tried to find the proper ways how we can improve the registration efficiency of dyed fission tracks in CN-85 viewed under normal light illumination. We have found that a replacement of the swelling step with a thermal annealing can increase both the efficiency and track width. According to the experimental data shown in Figs.1 and 2, an optimum of the annealing was found at 100°C for 1 hour. The existence of a maximum on the curve of Fig.1 may indicate a lateral diffusion of dyeable species without appreciable recombination up to 100°C and some sort of curing of the primary damage over 100°C.

The curves drawn on a semilogaritmic Gauss plot in Fig.3 may bring to certain light on the nature of the structural variation of the bulk of CN-85 sheets due to the annealing. Here we have shown the frequency distributions of the width of dyed tracks after different annealing conditions. As seen the

distributions indicate characteristic two-hump ourves where both humps can be well described by lognormal distribution. The percentage occurance of tracks in these humps varies with the duration of annealing. In our opinion, this effect may refleot the percentage inorease of the ratio of amorphous and crystalline regions in the CN-85 sheet with inoreasing annealing time.

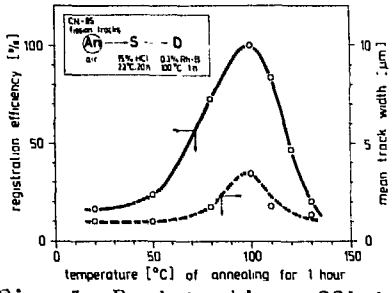

Fig. 1. Registration efficiency and mean width of dyed fission tracks at different annealing temperatures of latent tracks.

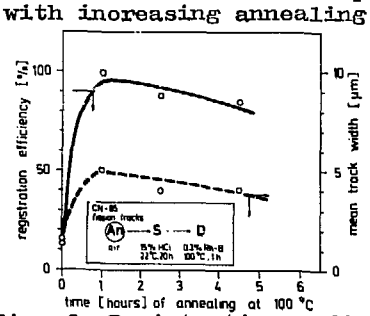

Fig. 2. Registration efficiency and mean width of dyed fission tracks at different annealing times of latent tracks.

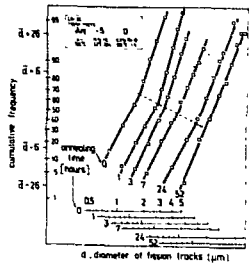

Fig. 3. Frequency distribution of the width of dyed fission tracks at different annealing times of latent tracks.

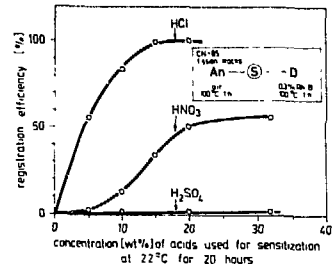

Fig. 4. Registration efficiency of dyed fission tracks when using different acids at different concentrations in the sensitization step.

In a second set of experiments we have tried to find the optimum sensitizing acid for CN-85. After irradiation the samples annealed under the optimum condition were immersed in water solution of hydrochloric, nitric and sulphuric acids of different concentrations. These experiments were carried out at 70°C for 1 hour and at 22°C for 20 hours, respectively. It was observed that at high sensitization temperature the dyed tracks became faint and diffuse whereas at room temperature they got deeper colour and high contrast. The results obtained at room temperature are shown in Fig. 4. As seen optimum condition can be achieved by 15% HCl and the use of H_2SO_4 practically does not give tracks. Further increase of the HCl concentration is not reasonable as an increasing density of some sort of inclusions (like gas bubbles) can be observed in the bulk of detector material.

In a third set of experiments the parameters of dyeing step were optimized (see Figs. 5 and 6). For the variation of the registration efficiency as a function of the dyeing parameters (temperature, time, dye concentration) similar trends were observed as in case of cellulose acetate (Somogyi et al, 1979a). Here, however, a much lower Rhodamine-B concentration (0.3% instead of 5 %) proved to be optimum.

Finally, we have started studies with electron-irradiated CN-85 sheets to simulate some basic behaviours of the dyed track method. Here, we assumed that a dominant role in the formation of active dyeable species (defects) might play the electrons produced along the tracks. A simulation study concerning the effect of annealing time and temperature on the dyeability of samples irradiated with 30 Mrad dose of 450 keV electrons is shown in Fig.7. The data indicate similar trends as observed for the dyed fission fragments (see Figs. 1 and 2). A more interesting result, the "dyeing response" of CN-85 as a function of the electron dose is presented in Fig.8. From this one

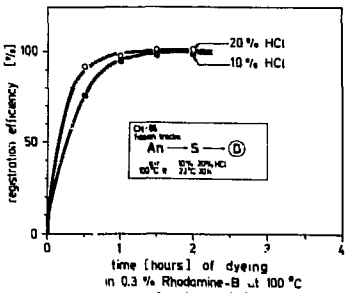

Fig. 5. Registration efficiency of dyed fission tracks when using different dyeing times.

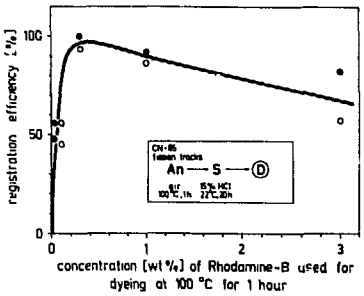

Fig. 6. Registration efficiency of dyed fission track when using different dye concentrations.

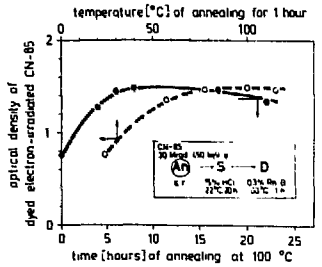

Fig. 7. Optical density of dyed electron-irradiated CN-85 sheet when using different annealing times and temperatures prior to sensitization and dyeing steps.

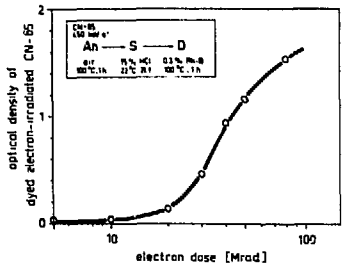

Fig. 8. Optical density of dyed electron-irradiated CN-85 sheet when using different doses of 450 keV electron beam.

can conclude that deeply coloured tracks (higher than 1 optical density) can be expected only for those particles which are able to deposit doses over 40 Mrad. One may consider about 20 Mrad as a threshold of dyed track visibility in CN-85.

REFERENCES

Lferde, M., J-L. Seidel, M. Monnin, G. Somogyi, and M. Tóth-Szilágyi (1982). Diffusion processes in dyed detectors. Proc. 11th Int. Conf. Solid State Nuclear Track Detectors, Bristol, Pergamon Press, 299-306.

Monnin, M., and G. Blanford (1973). Detection of charged particles by polymer grafting. Soience, 181, 743-744.

Monnin, M., J. Gourcy, G. Somogyi, and G. Dajkó (1980). Thermal stability of dyed tracks and electrochemical etching sensitivity of some polymeric detectors. Radiat. Phys. Chem. 15, 473-477.

Monnin, M., J. Gourcy, G. Somogyi, and M. Tóth-Szilágyi (1979). Non-etching track visualization: developments of the method. Proc. 10th Int. Conf. Solid State Nuclear Track Detectors, Lyon, Pergamon Press, 311-314.

Somogyi, G. (1976). Processing of plastic detectors. Proc. 9th Int. Conf. Solid State Nuclear Track Detectors, Munich, Vol.1. 255-284.

Somogyi, G., and M. Tóth-Szilágyi (1977). A new technique for track visualization, ATOMKI Közl. 19, 349-364.

Somogyi, G., M. Tóth-Szilágyi, M. Monnin, and J. Gourcy (1979a). Non-etching track visualization: some recent results. Proc. 10th Int. Conf. Solid State Nuclear Track Detectors, Lyon, Pergamon Press, 267-275.

Somogyi, G., M. Tóth-Szilágyi, M. Monnin, and J. Gourcy (1979b). Non-etching nuclear track visualization in polymers: fluorescent and dyed tracks. Nuclear Tracks. 3, 151-167.

ATOMKI Preprint E/4 (1983)

FORMATION OF ION-BEAM IMAGES IN GELATINE AND VARIOUS POLYMERS

G. Somogyi[*], I. Hunyadi[*], R. Ilić[**], A. Loose[**], and Zs. Varga[*]

[*]Institute of Nuclear Research of the Hungarian Academy of Sciences, H-4001 Debrecen, Hungary
[**]J. Stefan Institute, E. Kardelj University of Ljubljana, Yu-61000 Ljubljana, Yugoslavia

ABSTRACT

It has recently been reported by Najžer, Humar and Ilić (1982) that the pure gelatine can be used for producing relief images of high-fluence ion-beams after a treatment in water at room temperature for few minutes. The new method is proposed for high-resolution microradiography of boron in metals via $^{10}B(n,\alpha)^{7}Li$ reaction. In our present work studies are performed to understand the phenomenon observed. We have simulated the image formation by accelerated electron, proton and alpha-particle beams at different fluences. A narrow fluence region is found in which a highly enhanced dissolution rate of the irradiated gelatine is induced. We assume that when the fluence exceeds a critical value (tipically 10^{12}–10^{13} ions·cm^{-2}) the damage zones of individual tracks cover almost completely the irradiated area, transforming the irradiated layer into a huge damage zone. In this case the effective diameter of damage zone around a single track has to be $d_{eff} = \Phi_c^{-1/2} \simeq (3\text{-}10)$ nm. We have found that the ion-induced image formation phenomenon observed in gelatine is a more general one and the method may be extended to almost all the etch-track and non-etch-track forming polymers and perhaps to insulating silicates. For example, high-resolution α- microradiographs have been obtained with CR-39, CN-85, PC and PET sheets and even with hydrate-cellulose known as a non-track-forming material.

KEYWORDS

Microradiography, relief image, high spatial resolution, ion beams, radiation damage, latent track, enhanced dissolution, polymers.

INTRODUCTION

The purpose of our present work is twofold: i) to show that the development of a novel method for high-resolution microradiography is possible on the base of preferential dissolution of various dielectric solids covered with overlapping damage zones of nuclear tracks, ii) to present the main characteristics of the "multi-track autoradiography" by simulating the image formation with different accelerated nuclear particles.

The development of a high-resolution autoradiographic technique is desirable in many applications. The performance of high-quality images is, however, limited by various factors. These limits arise mostly from two sources. One is the finite dimension of the picture-forming unit element (pixel), e.g. the grain size in photographic emulsion or the dimension of etch-pits in dielectric track detectors, and the second is the statistical nature of the spatial emission of any particle sources (accelerated beam; radioactive source; neutron-, or ion-induced nuclear reaction) used in radiographic works. To overcome these limits such imaging technique is required which allows a significant reduction of the pixel dimension and "shot noise" fluctuation. The latter can obviously be achieved by the use of a high-fluence beam, i.e. by certain overexposure of the radiograph.

Recently Ilić and co-workers (1980) reported an interesting effect observed in a heavily neutron-irradiated Kodak-maximum resolution plate kept in contact with a boron-containing steel specimen. It is found that a non-photographic latent image of the boron distribution is formed in the gelatine of the plate, and this image can be transformed into a well-visible relief radiograph by soaking the film in pure water. This finding has shown a possible way of approach to the solution of the above-mentioned problem of high-resolution autoradiography. The high power of image detail discernment observed in gelatine (Najžer, Humar and Ilić, 1982) inspired the Ljubljana and Debrecen track detector groups to make common efforts to understand this ion-induced image formation phenomenon (Varga, Somogyi and others, 1983) and to develop a new neutron-induced, high-resolution radiographic technique for micromapping boron, uranium and gadolinium and for microneutronography (Loose, Hunyadi and others, 1983).

We have proved that the observed phenomenon is not restricted only to gelatine but can be extended to several etch-track and non-etch-track-forming dielectric solids as well. Some experimental results and theoretical considerations concerning this field of research is presented in this paper.

EXPERIMENTAL CONDITIONS

To study the basic characteristics of the phenomenon producing the ion-induced relief image, pure gelatine films and various polymer sheets (CR-39, CN-85, PC, PET, hydrate-cellulose) were subjected to alpha, proton and electron bombardment in a broad interval of particle fluences. To provide an aid to the comparison of the dissolution effects on the exposed and non-exposed areas, a fine metal grid was mounted on the surface of the samples to be studied. The experimental arrangement for the proton and alpha-particle exposures at the Van de Graaff generator of the Institute of Nuclear Research in Debrecen is shown in Fig.1. To produce a complete "radiographic response curve" (radiation effect versus particle fluence) in one run of irradiation along a stripe of the sample, a special set-up was designed in which we could cover about six orders of magnitude of fluences with the help of the Rutherford scattering of accelerated ions on a thin target of high atomic number. The electron irradiations were carried out at the Cocroft-Walton generator of our Institute in separated runs at each fluences.

The irradiated samples were immersed into water (or other solvents) for several minutes and dried. After this treatment the depth differences between the exposed and unexposed regions along the samples were measured by an electronic length measuring gauge mounted on the stage of a research microscope. The depth could be measured to a precision of 0.1 μm. The normalized residual thickness, $r = (t_o - t)/t_o$, was considered as a measure of the image-forming radiation effect in the sample, where t is the thickness of dissolved material layer and t_o is the total penetration length of the bombarding ion. Other experimental details see in the paper by Varga et al. (1983).

RESULTS

The typical shape of the "radiographic response curve" characteristic of gelatine films is shown in Fig.2. One can see that there is a considerable difference in the radiation-enhanced dissolution sensitivity observed by us for the two films of different origin. The gelatine film type I of 40 μm thick made by a Yugoslavian firm shows a more compact structure and lower sensitivity. The film type II of 10 μm, prepared in our laboratory (5 g gelatine dissolved in 250 cm^3 water at 50 °C, poured on a glass plate and solidified), is more sensitive.

Similar radiation response characteristics have also been observed for CN-85 and hydrate-cellulose when using water and/or solvants (e.g. ethanol) for the heavily irradiated surfaces. Such examples of observations are illustrated in Fig.3 showing the effect of high alpha-particle fluences on the water dissolution behaviour of CN-85 and hydrate-cellulose films. It is interesting to note that the first film is known as a material which is able to form etchable single tracks, but the second one is not an etch-track

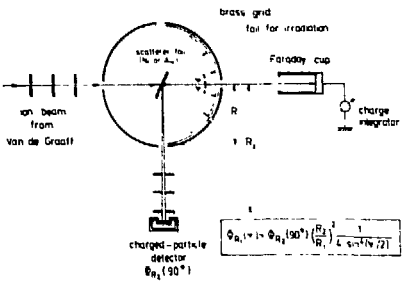

Fig.1. Exposure arrangement for providing the "radiographic response curve" of gelatine and plastics for protons and alphas.

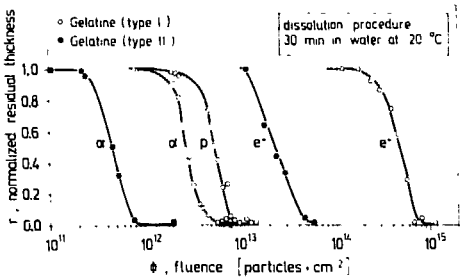

Fig.2. "Radiographic response curves" of gelatine films for 3.5 MeV alphas, 2 MeV protons and 0.45 MeV electrons.

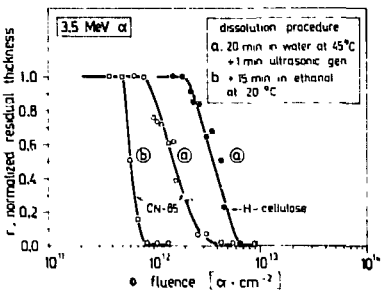

Fig.3. "Radiographic response curve" of an etch-track and a non-etch-track forming film (CN-85 and hydrate-cellulose) for 3.5 MeV alphas.

forming film. Some microphotographs illustrating the appearance of typical relief images under different conditions are shown in Fig.4. We have also succeeded in revealing relief images in CR-39, PC and PET sheets, applying a short treatment in diluted basic solutions.

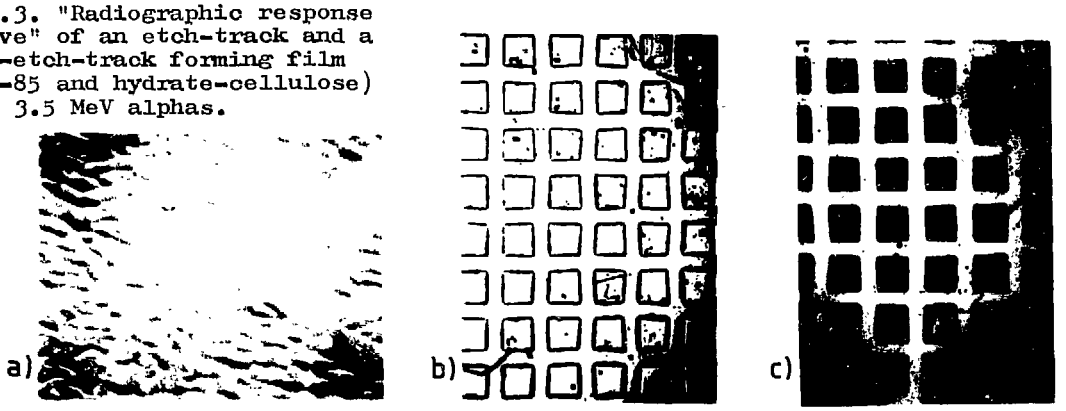

Fig.4. Relief images dissolved by water in various solids; a) gelatine, boron distribution in steel via $^{10}B(n,\alpha)$ reaction (22°C water, 30 min.), b) CN-85, grid imaging by 3.5 MeV α-beam (50°C water, 20 min.), c) hydrate-cellulose, grid imaging by 3.5 MeV α-beam (50°C water, 20 min. +Methylene-blue).

DISCUSSION AND THEORETICAL CONSIDERATIONS

From our present results it is obvious that i) the phenomenon found by Ilić et al (1980) in gelatine is a preferential ion-induced dissolution over a critical fluence and ii) it should be a more general process which may be observed in almost all the insulating materials (in polymers and perhaps even in glasses and minerals). Consequently, the field of its application to high-resolution radiography via certain nuclear processes should also be quite broad. Such possibilities found by us are presented in another contribution at this conference (see Loose, Hunyadi and others, 1983). Here, we try only to analyse the shape of experimental response curves and to give a possible explanation of the phenomenon observed.

We have found that the shape of response curves can be excellently described by the relation

$$r^{-1} = 1 + (\phi/\phi_{0.5})^{n}, \qquad (1)$$

where $\phi_{0.5}$ is the half-thickness fluence, $n=\gamma\cdot 4\ln 3/\ln 10 = 1.9\gamma$, and γ, the slope of the curve at $\phi = \phi_{0.5}$, is a measure of the contrast ratio of relief images. This ratio can be expressed by the relation

$$\gamma = \left[\log \phi_{0.9}/\log \phi_{0.1}\right]^{-1} \qquad (2)$$

where $\phi_{0.9}$ and $\phi_{0.1}$ denote the particle fluences required to get 90% and 10% residual thickness of the penetration depth of the bombarding particles in a given material. For all the cases studied, the contrast ratio is found to be in the interval of 1.7-3.3. The corresponding $\phi_{0.9}/\phi_{0.1}$ values run from 4 to 2.

Some response curves calculated by the relation (1) at different contrast ratios are shown in Fig.5. One can see the following main characteristics: i) at low fluences there is no observable dissolution effect, then appears a very low dissolution rate varying slowly with the increase of fluence, ii) over $\phi_{0.9}$ abruptly a very steep variation in the dissolution of the irradiated region can be observed, iii) finally the effect reaches a saturation over a critical fluence of about $\phi_c = \phi_{0.1} = (2\text{-}4)\phi_{0.9}$.

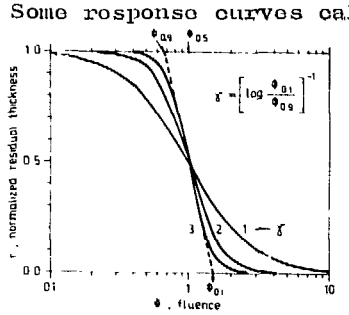

Fig.5. "Radiographic response curves" calculated by Eq. (1) at different contrast ratios, γ, assuming $\phi_{0.5}=1$.

Here the question arises what a phenomenon can be responsible for the abrupt appearance of such a greatly enhanced dissolution effect between $\phi_{0.9}$ and $\phi_{0.1}$ which results in a very high spatial resolution of the observed relief images. The degree of ion-beam modification (M) of a polymer may depend i) on the dose (D) deposited by the ions in the bombarded area ii) on the efficiency of radiation chemical transformations (G-value) and iii) on the rate of preferential solubility (S) induced by unit chemical transformation. Finally the resulting effect is $M = D\cdot G\cdot S$ where $D = D_1 P = D_1 \phi d^2\pi/4$. Here ϕ is the number of impinging ions on a unit area, d is connected to the diameter of a cylindrical damage zone around the latent track where most of the single particle dose D_1 is practically concentrated, and P is the nominal probability of areal cover by such cylindrical unit cells of the latent tracks.

TABLE 1 Probability of the occurence of single, double and multiple track configurations at different nominal (P) and effective (P_{eff}) probability of areal cover.

$P = \phi\cdot d^2\pi/4$	0.1	0.18	0.78* = π/4	1	2
$P_{eff} = 1-\exp(-P)$	0.095	0.165	0.54	0.63	0.86
$P_1 = \exp(-4P)$	0.67	0.49	0.043	0.018	0.00
$P_2 \simeq 4P.\exp(-5.645P)$	0.23	0.26	0.037	0.014	0.00
$P_{n\geq 3} = 1 - P_1 - P_2$	0.10	0.25	0.92	0.97	0.99

*in this case $\phi\cdot d^2 = 1$; ϕ = track fluence, d= effective diameter of single damage zones

We assume that the abruptly enhanced material dissolution may appear in a range of ion fluences where the percentage cover of the exposed area by the damage zones of numerous single tracks becomes significant and the percentage overlap of these zones starts to grow to a great extent. We have tried to predict the region of the appearance of such effect by using the relations by Riedel and Spohr (1981) and Somogyi and Dajkó (1980) for describing the coincidence of statistically distributed circular damage areas ($d^2\pi/4$) as a function of their areal densities (ϕ). The resulting probabilities for finding single-hit (P_1), double-hit (P_2) and multi-hit ($P_{n\geq 3}$) damages are shown in Table 1 at few typical values of the nominal probability of areal cover, P. One can see that the probability of the occurence of partially overlapping multiple track configurations is abruptly increasing over

P=0.18, then it practically reaches a saturation (92%) at about P = $\pi/4$ value. We note that in the latter case the $\phi_c d^2=1$ condition is exactly satisfied. The ϕ_c critical fluence defined by this relation can be considered as a minimum fluence for correct exposure in the high-resolution radiography. It is interesting to note that the $\phi_c d^2= 1$ condition represents the ideal case of a completely full array of equidistant touching damage zones. Taking into consideration the typical experimental values of $\phi_c= 10^{12}$-10^{13} ions/cm^2, one can find that the effective damage of light ions in polymers has to be restricted to a zone of about 3-10 nm in diameter. Assuming that $\phi_{0.9}$ is at P=0.18 and $\phi_{0.1}$ at P=0.78 we can get a value of 1.6 for the contrast ratio (γ) in reasonable agreement with the typical observations.

CONCLUSION

We have demonstrated that a very high resolution radiography can be performed in gelatine and in several etch-track and non-etch-track forming polymers over a critical high value of particle fluence. We have shown that the appearance of such image-forming phenomenon (abrupt enhanced dissolution) can be explained by a multi-hit damage process. Our studies strongly suggest that the presented phenomenon should be a very general one and its radiographic application may be extended to all the dielectric solids including even silicates. The existence of such a preferential dissolution of ion-implanted soda-lime glass in saline solution has already been demonstrated very recently by Lanford and Burman (1983)

REFERENCES

Ilić, R., M. Humar, M. Najžer, and A. Podgornik (1980). Heavy charged particle autoradiography using Kodak maximum resolution plate. Proc. 10th Int. Conf. Solid State Nuclear Track Detectors, Lyon, Pergamon Press, 689-693.

Lanford, W.A., and C. Burman (1983). Effect of ion implantation on the reaction between water and glass. Nucl. Instr.Meth. 209/210, 1099-1103.

Loose, A., I. Hunyadi, G. Somogyi, Zs. Varga, M. Majžer, and R.Ilić (1983). Neutron-induced autoradiography based on relief and dyed image formation in polymers. Proc. 12th Int. Conf. Solid State Nuclear Track Detectors, Acapulco, present issue.

Najžer, M., M. Humar, and R.Ilić (1982). Microautoradiography with gelatine. Proc. 11th Int. Conf. Solid State Nuclear Track Detectors, Bristol, Pergamon Press, 77-80.

Riedel, C., and R.Spohr (1981). Correcting overlapping counts in dose calibrations at high event-density, GSI-81-2, Darmstadt, p.179.

Somogyi, G., and G. Dajkó (1980). A proposal for spark counting at high track densities. Proc. 10th Int. Conf. Solid State Nuclear Track Detectors, Lyon, Pergamon Press, 371-380.

Varga, Zs., G. Somogyi, I. Hunyadi, R. Ilić, and A. Loose (1983). Ion-beam images in gelatine. Proc. 13th Int. Symp. on Autoradiography, Tábor, (Czechoslovakia), in press.

ATOMKI Preprint E/5 (1983)

STUDY OF SPOT DEVELOPMENT AROUND TRACK- AND ELECTRIC-TREE--INDUCED PERFORATIONS THROUGH AN ALUMINIZED TRACK DETECTOR

G. Dajkó and G. Somogyi

Institute of Nuclear Research of the Hungarian Academy of Sciences, H-4001 Debrecen, Hungary

ABSTRACT

Recently, a new method for electrochemical etching of fission and alpha--tracks in thin aluminized plastic detectors was proposed by Tommasino et al. (1982 a,b). By using the new ECE-method, the electric-tree-induced perforations through nuclear tracks in plastic foils are non-shorting with aluminium at positive polarity, due to an isulating anodic oxid formation. Therefore, a fast dissolution of the aluminium layer by basic electrolyte can be avoided. We have studied the main trends of the growth of mean diameter of spots dissolved around fission tracks in aluminized PET foils as a function of the strength of electric field, frequency of voltage and time of etching in 30% KOH, with using both DC and AC voltages and without using field. It is proved that the electric field greatly enhances the rate of etching along the tracks. With irradiation under vacuum a considerable delay in spot appearance is observed. This effect can be partially reduced by using a regeneration period in air after irradiation. The spot diameter distribution obtained by the new ECE-method can be described by the sum of two curves of lognormal distribution, corresponding to the light and heavy fission tracks.

KEYWORDS

Nuclear track detector; new electrochemical etching; aluminized polyester; track- and tree-induced foil perforation; anodic oxidation; fission fragments.

INTRODUCTION

A method based on etched-through tracks in a thin aluminized detector foil for enlarging tracks and improving the counting condition was first suggested by Fleischer et al (1966). Here the detector is kept in a two-compartment device and the foil is etched through along the tracks from the non-aluminized side. After perforation, the reaction taking place between the aluminium and the penetrating etching reagent results in a bright, aluminium-free area (henceforth spot) surrounding the track holes. A modified, improved version of such a track enlarging method is proposed recently by Tommasino et al (1982a,b), which overcomes certain limitations of the former one. The method, called new electrochemical etching (henceforth NECE), makes use of low DC or AC voltages during the etching process. An important novelty of the NECE is that the track--induced perforations in the thin foil are non-shorting due to the formation of a ring-shaped aluminium oxide layer around the end of track channels.

The aim of our present work is to study the behaviour of spot growth in the NECE technique under various experimental conditions. Such studies should be useful from both practical and theoretical aspects. Here, the spot overlapping may be considerably reduced, and even short-range particles (shorter than foil thickness) may be registered with large size when using the NECE with AC voltage. It is also hoped that such studies may help the understanding of the already complex problem of the normal ECE process.

EXPERIMENTAL PROCEDURE

The experimental apparatus used in our studies is practically the same as developed for our normal ECE studies (Somogyi, 1977). As detector, a 10 μm thick polyester (PET) foil is applied. The irradiated foil is mounted on the circular opening of the etching vessel in such a way that the aluminized surface be in contact with the air and with a power supply of variable voltage (max 50 Volt). The inner compartment of the vessel is then filled up with the etchant electrolyte (30% KOH) and kept at room temperature.

For the sake of simplicity, our systematic studies were carried out with the tracks of fission fragments originating from a ^{252}Cf source. The irradiations were mostly performed in air in 2π-geometry. In some cases, however, collimated beams in an evacuated chamber were also used (e.g. in case of Fig. 6). After completing the NECE, the diameters of bright spots around the track endings were measured under a projection microscope with about 1 μm precision and their distribution and mean value were determined.

RESULTS AND DISCUSSION

At given moments during the NECE process, the thin PET foil is perforated along the individual tracks and the basic etchant starts to form aluminium oxide rim around each of them. This self-healing process starts to reduce the rate of etchant penetration to the unattacked aluminium layers. Consequently, the appearance of a saturation in the growth of spot sizes can be expected. It is also obvious that the spot sizes will be not identical for different tracks as the "retardation time" of spot formation (spot induction time) should be dependent on the length of track portions intersecting the thin detector. Therefore, in a thin detector irradiated in 2π-geometry, the spot size should have a given spread due to the angle-dependent length of track portions. In our first experiments these questions were studied. Both the visual observations (Fig.1a) and spot-size measurements (Fig.1b) indicated that spots do really display a relatively broad size spectrum, but surprisingly with two peaks possessing lognormal distorbution, in which the number of spots is about the same. We have found that these two peaks appear always in the spot diameter distribution independently on the angle of irradiation (practically between 90-45°C for our 10 μm thick foil) under the used experimental conditions. (We note here that in these latter experiments we eliminated the so-called "vacuum effect" discussed at the end of the section.) These results strongly suggest that the two peaks should correspond to the tracks of heavy and light fission fragments. In addition, this finding indicates that the spot inductions and formation time in the NECE technique should be fairly sensitive to the variation of radiation damages to make the development of a new particle identification technique possible.

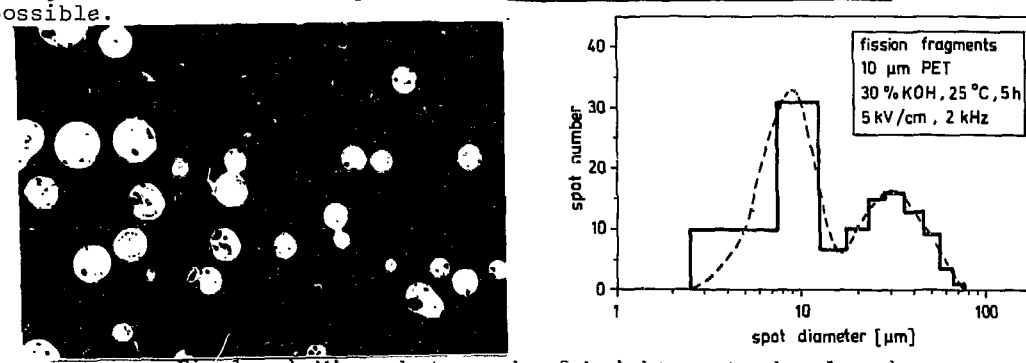

Fig.1. a) Microphotograph of bright spots developed around fission tracks by NECE and b) a typical spot diameter distribution in an irradiation of 2π-geometry.

In a second set of experiments we have studied the characteristics of the variation of mean spot diameter as a function of the duration of etching in different electric fields. Each point of these curves was obtained from the mean value of the spot diameters observed at the tip of 100 individual tracks. The results, shown in Fig.2 clearly indicate the large differences between the

effects originating from the AC, DC and "no field" conditions. In these cases the spot growth starts after different induction times, corresponding to the different penetrability of the etchant into the track portions crossing the detector. The most stricking etch-rate enhancement effect is produced by the use of AC voltage. The smallest saturation spot diameters can be obtained with DC voltage which should have of practical importance in case of higher track densities to reduce the overlap of tracks.

We have tried to measure the etch-rate enhancement directly along the fission tracks in a thicker (100 μm) PET foil. For this purpose, an irradiated foil was cut for two pieces, and one of them was etched in a normal ECE device by using relatively low field strength (20 kV/cm) while the second piece with using no field. We have measured the mean length of such tracks ($\theta \leq 30^{o}$ to the surface) which could not form "discharge-spots" under our experimental conditions. The results shown in Fig.3 clearly indicate a considerable enhancement of the track etch-rate even for the very obliquely entering particles. This enhancement should be induced by the highly inhomogeneous electric field in the very thin and pointed channels of the etched tracks, and consequently the effect should increase toward right angle. Finally, one can conclude that the rate of etchant penetration should be dominantly governed by the dielectrophoretic force induced by the high and very inhomogeneous field (Pohl, 1958), as we had proposed earlier for a very similar etching condition (Somogyi and Almási, 1982).

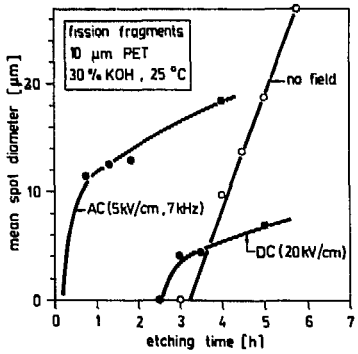

Fig.2. Dependence of the mean spot diameter on the etching time under different "fields"

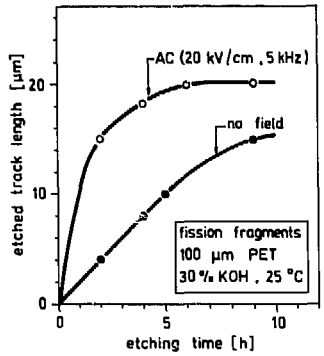

Fig.3. Dependence of the length of fission tracks on the etching time using field and no field.

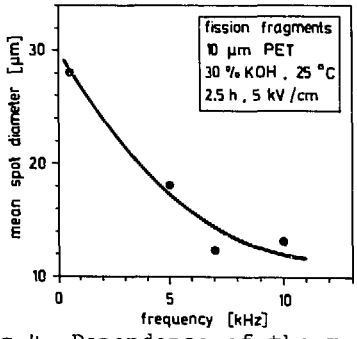

Fig.4. Dependence of the mean spot diameter on the frequency of voltage.

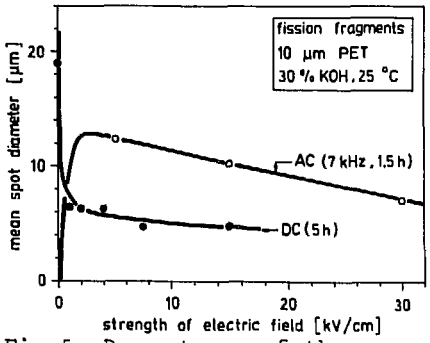

Fig.5. Dependence of the mean spot diameter on the strength of electric field.

In order to get additional data on the self-healing phenomenon we have examined the effect of the main electric parameters (frequency, field strength) on the spot development. Some preliminary results obtained are presented in Figs. 4 and 5. The data in Fig. 4. show that at higher frequences the self-healing is more effective, that is the insulating and non-etchable aluminium oxide layer grows faster. It may be noted that this conclusion seems to be inconsistent with the results shown in Fig. 5. where the effect of the change of field strength is demonstrated at particular set of parameters. In Fig. 5 the self-healing seems to be more effective at low frequency (more exactly at DC

where the frequency is zero). This contradiction can be resolved by the assumption of the existence of a maximum on the curve in Fig. 4 below 1 kHz. As a result it has become clear that it is worth extending the studies to the low-frequency region as well. From Fig. 5 it can also be concluded that the spot growth displays a saturation effect and the spot diameter is hardly sensitive for the variation of field strength above a particular value (≈2 kV/cm).

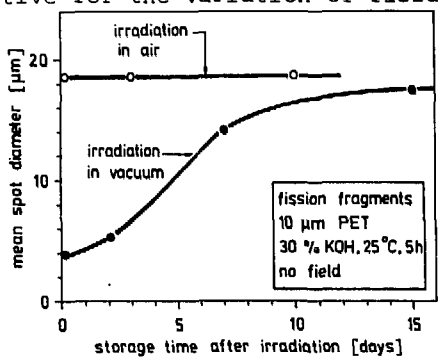

Fig.6. Spot diameter as a function of the storage time elapsed between the irradiation and etching for different irradiation conditions.

Finally, we should pay some sentences to the strong "vacuum effect" observed in some of our experiments related to NECE. We have found that, in agreement with the statement reported in an early work by Monnin (1968), a considerable delay emerges in the formation of etched tracks, and consequently in the spot growth too, if the irradiation of PET foil by fission fragments is carried out in a vacuum chamber. Our studies have proved that the effect is reversible (see Fig 6). The storage time required for almost full regeneration, however, is very long (two weeks for our foil). This effect should be related to the presence or absence of oxygen in the damage zone.

REFERENCES

Fleischer, R. L., P. B. Price, and R. M. Walker (1966). Simple detectors for neutrons and heavy cosmic ray nuclei. Rev. Sci. Instr. 37. 525-527.

Monnin, M. (1968). Etude de l'interaction des particules lourdes ionisates avec les macromolecules a l'etat solide. PNCF68-RI9. Universite de Clermont.

Pohl, H. A. (1958). Some effects of nonuniform fields on dielectrics. J. Appl. Phys. 19, 1182-1188.

Somogyi, G. (1977). A study of the basic properties of electrochemical track etching. Rad. Effects, 34, 51-56.

Somogyi, G. and Gy. Almási (1982). Study of the electric treeing produced around nuclear tracks by SEC-treatment. Proc. 11th Int. Conf. Solid State Nuclear Track Detectors, Bristol, Pergamon Press, 245-249.

Tommasino, L., G. Zapparoli, and F. Caiazzo (1982a). A new method for electrochemical etching: I. Results with dc voltage. Proc. 11th. Int. Conf. Solid State Nuclear Track Detectors, Bristol, Pergamon Press, 211-214.

Tommasino, L., G. Zapparoli, and F. Caiazzo (1982b). A new method for electrochemical etching: II. Results with ac voltage. Proc. 11th. Int. Conf. Solid State Nuclear Track Detectors, Bristol, Pergamon Press, 215-219.

ATOMKI Preprint E/6 (1983)

CALCULATION OF THERMAL EFFECTS OCCURING DURING THE MANUFACTURE OF CR-39 SHEETS

S. Szilágyi and G. Somogyi

Institute of Nuclear Research of the Hungarian Academy of Sciences, H-4001 Debrecen, Hungary

ABSTRACT

To manufacture a good-quality, uniform CR-39 track detector, the polymerization rate should be chosen below a critical value to avoid the development of undesirable thermal gradients and internal temperature fluctuations in the sheet being cast. To improve curing cycles, especially for thick CR-39 sheets, a computer programme was developed by which we could study the trends of thermal effects under different casting conditions. Our calculations are based on the solution of the one dimensional heat transport equation, taking into account the relations proposed by Dial et al (1955) for describing the chemical kinetics of CR-39 polymerization. We have revised the empirical parameters available to such calculations. With new "Dial constants" we have calculated the critical initial bath temperature (which results in thermal runaway at the central plane of the sheet being cast) as a function of the CR-39 thickness and IPP initiator concentration. Results are also presented for the temperature profile developing in the depth of cast CR-39 sheets.

KEYWORDS

CR-39 plastic; polymerization; thermal effects; track detector.

INTRODUCTION

The heat release in the polymerization of CR-39 is extremely high (~130 kJ/mole), especially at the beginning of curing process. Therefore, if the initial curing temperature is too high, the thermal gradients evolved in the monomer might give rise to non-uniform polymerization, consequently to non-uniform track response in the depth of cast sheet. In extreme cases, this effect is so high that the shock due to the "thermal runaway" of polymerization is able to shatter the glass molds.

In commercial grade CR-39 products we encounter frequently the problem of non-reproducibility and non-uniformity in both track and bulk etching responses in depth and even from sheet to sheet. This presents serious difficulties in several applications of CR-39 as nuclear track detector. Therefore, to learn the correct rules of the production of uniform detector material, studies concerning the behaviour of internal temperature excursions should have of fundamental importance.

Although few works have been reported on the problem of heat release and transfer during manufacture of CR-39 (Fowler et al, 1980; Adams, 1982; Somogyi, 1982; Turner et al, 1982), to date there has been no systematic, quantitative study published on the dependence of critical initial and internal sheet temperatures on the main polymerization parameters. In the literature, only illustrative examples have been published on the thermal runaway as a potential source of track response variations with depth in the cast sheet (Fowler et al, 1980; Turner et al, 1982).

Taking into account the chemical kinetics of CR-39 polymerization described first by Dial and others (1955) and a theoretical consideration

concerning the heat release and thermal conductivity in a slab-shaped CR-39, we have developed a computer programme to calculate the main trends of the variation of internal CR-39 temperature. By this programme our original aim was to device proper external (bath) temperature versus curing time cycles that maintain small temperature gradient in the sheet (Somogyi, 1982). Simultaneously, similar efforts have been made by Turner and coworkers (1982) and Adams (1982).

In this work we present some results of our calculations to show some typical effects due to the high heat release during polymerization. The following relationships are considered: critical initial bath temperature, T_{oc}, (which results in thermal runaway at the centre of the sheet being cast) as a function of the IPP initiator concentration (c) and sheet thickness (h); dependence of the internal CR-39 temperature, $T_{h/2}$ (which is evolved at the centre of the sheet), on curing time (t); and the variation of sheet temperature (T) with depth at different curing times.

PRINCIPLE OF CALCULATION

To study the internal temperature effects during CR-39 polymerization we have taken into consideration i) the characteristics of the chemical kinetics and ii) that of the production of heat and its transfer by thermal diffusion.

i) According to the results of Dial and others (1955), the rate of CR-39 polymerization and the change of monomer and initiator concentration during the curing process can be described by the equations

$$-\partial m/\partial t = m\, c^{1/2} Z_3 \exp(-E_3/RT), \qquad (1)$$

$$\partial m/\partial c = Z_1 \exp(-E_1/RT) \qquad (2)$$

where $\underline{m}$ and $\underline{c}$ are the monomer and initiator (IPP) concentrations normalized to their initial values, T is the temperature of CR-39 after $\underline{t}$ curing time, and Z_1, Z_3, E_1, E_3 are constants fitted by Dial et al (1955) to experimental data.

After a revision of the original value of "Dial constants" (Z_1=0.043, Z_3=$3.51\cdot10^{18}h^{-1}$, E_1=-4.41 Kcal/mol, E_3=29.05 Kcal/mol) we have found that, by using R=8.30 J/mol·K value, best fit to Dial's results can be actually obtained by the following new set of data: Z_1=0.044, Z_3=$1.75\cdot10^{18}h^{-1}$, E_1=-4.32 Kcal/mol and E_3=28.55 Kcal/mol. In our calculations we have used the above constants with the exception of the value of E_3, for which 28 and 29 Kcal/mol were chosen to show the influence of the accuracy of its measured value on the calculated thermal characteristics (see later). These constants and all the other parameters used in our calculations are summarized in Table 1 in terms of SI-units.

TABLE 1 Summary of the data, related to CR-39 properties, used in our calculations.

Thermal conductivity for		
monomer	λ_m	= $1.045\cdot10^{-3}$ J/(cm·K·s)
polymer	λ_p	= $2.09\cdot10^{-3}$ J/(cm·K·s)
Specific heat for		
monomer	c_m	= 1.21 J/g·K
polymer	c_p	= 2.3 j/g·K
Specific density (20/4°C)		
monomer	ρ_m	= 1.143 g/cm^3
polymer	ρ_p	= 1.32 g/cm^3
Molecular weight	M	= 274.3 g/mol
Diffusion coefficient $D=\lambda_m/(c_m\cdot\rho_m)$		= $7.52\cdot10^{-4}$ cm^2/s
Molar gas constant	R	= 8.30 J/mol·K
"Dial constants"	Z_1	= 0.044
(for using IPP)	Z_3	= $4.86\cdot10^{14}$ s^{-1}
	E_1	= - 18.1 kJ/mol
	E_3	= 121.2 kJ/mol (or 117.C kJ/mol)
Heat of polymerization $Q=(E_1+E_2)/M$		= 103.1 kJ/mol (or 98.9 kJ/mol)

ii) Considering a large CR-39 plate of $\underline{h}$ thickness, in which Q heat of polymerization is produced, the differential equation describing the T(x,t) temperature distribution in a given $\underline{x}$ depth under the plate surface at $\underline{t}$ curing time, can be given by the one dimensional heat transport equation

$$\frac{\partial T}{\partial t} = D\frac{\partial^2 T}{\partial x^2} + \frac{Q}{c_m}\frac{\partial m}{\partial t} \qquad (3)$$

where D and c_m are defined in Table 1. For the solution of such type of differential equation, taking into account equations (1) and (2) also, only numerical methods are known. To get the T(x,t) function under given boundary conditions (sheet thickness, initial bath temperature, initiator concentration) we have adopted the calculation procedure described by Meis and Marcowitz (1981). The programme was run at a PDP-11/40 computer.

RESULTS AND DISCUSSION

As a first task we have made calculations concerning the influence of initiator concentration on the condition of appearance of thermal runaway at various CR-39 thicknesses. As Fig.1 shows, the critical initial temperature of water bath (in which the mold is immersed during the curing process) is a slowly decreasing function of the increasing IPP concentration. A much more pronounced effect is produced by the increase of the thickness of the sheet to be cast. According to our calculations, using the parameters in Table 1, the thermal runaway can appear even at room temperature for thicker sheets (see Fig.2). Practical experiences have shown that this phenomenon actually starts

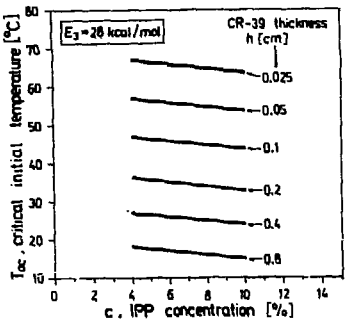

Fig.1. Variation of critical bath temperature (resulting in thermal runaway) with initiator concentration for different CR-39 thicknesses being cast. Note: the parameters used in the calculations, and not indicated in the Figure, are summarized in Table 1.

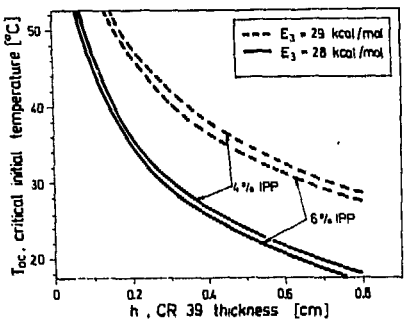

Fig.2. Variation of critical bath temperature with CR-39 thickness at different initiator concentrations, using different E_3 values in the calculations. (See note in Fig.1.)

to appear only at a curing temperature over 40°C for sheets thicker than 8 mm. We have tried to change the value of E_3 in our calculations to find a better agreement with the observations. It was found that a 4% increase in E_3 (using 29, instead of 28 Kcal/mol) can give rise to a 10°C increase in T_{oc} (see the dotted lines in Fig.2). This finding clearly indicates that much more accurate determination of the "Dial constants" is required, as certain calculations might be extremely sensitve even for small alterations of the parameters of calculation. It is interesting to note that with a further increase of the value of E_3 the calculated T_{oc} values show a maximum, then at about E_3=34 Kcal/mol the results become similar to those represented by the solid lines in Fig.2. A reasonable agreement with the observations might be obtained with a value of about 30.5-31 Kcal/mol.

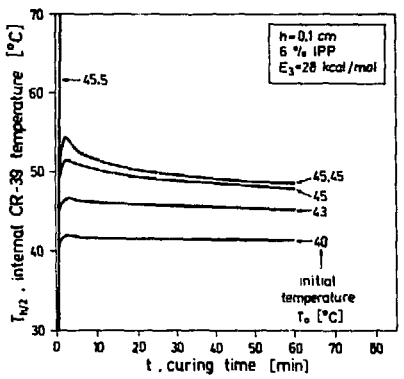

Fig.3. Calculated curves showing the internal CR-39 temperature as a function of curing time at different initial bath temperatures for a "thin" sheet. (See note in Fig.1.)

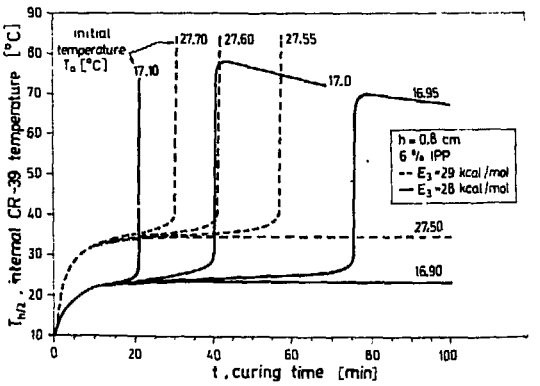

Fig.4. Internal CR-39 temperature curing time plots at different initial bath temperatures for a "thick' sheet, using different E_3 values in the calculations. (See note in Fig.1.)

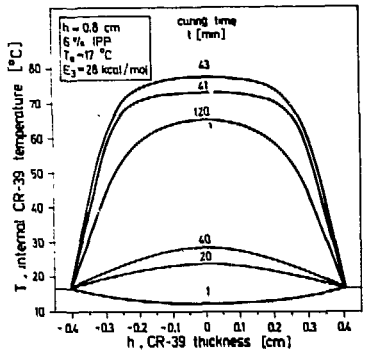

Fig.5. Calculated curves showing the variation of internal CR-39 temperature with depth in a "thick" sheet at different curing times, when the bath temperature is just below the critical one (T_{oc}-T_o= =0.1°C). (See note in Fig.1.)

In spite of keeping the T_o bath temperature at a constant value at the beginning of curing cycle, inside the sheet somewhat higher temperature will occur. To manufacture a uniform detector material, the initial curing temperature should be kept sufficiently low to have only 1-2°C temperature gradient between the surface and central plane of the sheet. To device such a cycle, the dependence of internal CR-39 temperature, $T_{h/2}$ (at half sheet thickness), on the curing time is required at different initial (bath) temperatures. In Figs.3 and 4 such calculated curves are presented for a "thin" and a "thick" sheet. As can be seen the thermal runaway appears very suddenly in a relatively narrow interval of the initial temperature in agreement with the experimental observations (Turner et al. 1982). In Fig.4 we also illustrate, as in Fig.2, the effect of the change of the value of E_3 on the position of calculated curves.

Finally, we have studied the theoretically excepted shape of the depth dependence of internal temepratures around the central plane of a thick CR-39 sheet. An example of such calculations is shown in Fig.5. Although the value of E_3 parameter used here is not realistic, the curves well illustrate the appearance of a steep thermal gradient (and consequently a very non-uniform track response) in the depth under a curing condition which is not far from a thermal runaway.

CONCLUSION

Our calculations using revised "Dial constants" have shown that the heat production and transfer during CR-39 polymerization can be described more correctly with assuming a polymerization heat higher than the usual one quoted in the literature. In addition, we have pointed out that the IPP concentration is not, but the thickness of the sheet is very determining factor in choosing the permissible initial curing temperatures for production of uniform CR-39 track detectors.

REFERENCES

Adams, J. H. (1982). A curing cycle for detector-quality CR-39. Proc. 11th Int. Conf. Solid State Nuclear Track Detectors, Bristol, Pergamon Press, 145-148.

Dial, W. R., W. E. Bissinger, B. J. Dewitt, and F. Strain (1955). Polymerization control in casting a thermosetting resin. Industrial and Engineering Chemistry, 47, 2447-2451.

Fowler, P. H., V. M. Clapham, D. L. Henshaw, D. O' Sullivan, and A. Thompson (1980). The effect of temperature-time cycles in the polymerisation of CR-39 on the uniformity of track response. Proc. 10th Int. Conf. Solid State Nuclear Track Detectors, Lyon, Pergamon Press, 437-441.

Meis, T., U. Marcowitz (1981). Numerical solution of partial differential equations, Appl. Math. Sciences. 32, Springer-Verlag New York Inc. pp. 459.

Somogyi, G. (1982). Status of development in the field of CR-39 track detectors. Proc. 11th Int. Conf. Solid State Nuclear Track Detectors, Bristol, Pergamon Press, 101-113.

Turner, T. W., V. M. Clapham, A. P. Fews, and D. L. Henshaw (1982). On the quantitative analysis and effects of internal temperature fluctuations during cure of the polycarbonate CR-39. Proc. 11th Int. Conf. Solid State Nuclear Track Detectors, Bristol, Pergamon Press, 141-144.

ATOMKI Preprint E/7 (1983)

NEUTRON-INDUCED AUTORADIOGRAPHY BASED ON RELIEF AND DYED IMAGE FORMATION IN POLYMERS

A. Loose[x], I. Hunyadi[xx], G. Somogyi[xx], Zs. Varga[xx], N. Najžer[x] and R. Ilić[x]

[x]J. Stefan Institute, E. Kardelj University of Ljubljana, POB 53, 61111 Ljubljana, Yugoslavia
[xx]Institute of Nuclear Research of the Hungarian Academy of Sciences, P.F. 51, H-4001 Debrecen, Hungary

ABSTRACT

Neutron-induced autoradiography utilizing formation of a dyed and/ or relief image in polymers was developed. The method is based on the detection of neutron-induced charged particles, via (n,p), (n,α), (n,f) reactions and those neutron capture processes leading to internal conversion and/or β-decay. Irradiated polymers are treated in water containing an organic dye or in pure water for a few minutes to obtain a dyed and/or relief image, respectively. The fluence of charged particles required to produce a dyed image is between 10^{11} – 10^{12} cm^{-2} which is one order of magnitude less than that for a relief image. Various procedures based on utilization of optical and electron microscopy for contrast enhancement were developed. The techniques were applied to image boron, uranium and gadolinium in solids. Samples were irradiated in the core of a nuclear reactor. The required thermal neutron fluence was between 10^{14} – 10^{16} cm^{-2}.

KEYWORDS

Autoradiography; boron; dyed image; gadolinium; gelatine; image processing; polymers; relief image; solid state nuclear track detectors; uranium.

INTRODUCTION

Generally, formation of a Neutron-Induced Autoradiographic (NIA) image in polymers is associated with chemical etching of latent tracks (Fowler and Clapham,1982). Previously we have reported a new NIA technique using pure gelatine as an image detection material (Ilić and others, 1980; Najžer, Humar and Ilić, 1982). It was found that the latent image created at a high fluence of $^{10}B(n,\alpha)$ reaction products of $\sim 10^{12}$ cm^{-2} can be transformed to a visible negative relief image upon soaking the irradiated gelatine layer in pure water and subsequent drying in air. We have continued our studies and recently found that a stable negative relief image on gelatine can also be obtained by electrons and protons (Varga and others, 1983). Our most recent studies showed that this image formation phenomenon is more general and was found in some other etch-track and non-etch-track polymers (Somogyi and co-workers, 1983). The mechanism of the relief image formation, its theoretical description and the exposure characteristics of various polymers to different charged particles are given in an accompanying paper at the present Conference (Somogyi and co-workers, 1983).

In the course of this study, we substituted for water an organic dye such as methylene blue, and observed that a dyed image is formed at a fluence which is lower by approximately one order of magnitude than that required for a relief image. On the basis of these phenomena, new NIA techniques are proposed and described in the present work. The applicability of the technique for the determination of boron, uranium and gadolinium using gelatine and hydrate cellulose is investigated. Suggestions are made for further development of the techniques for imaging isotopes having high cross sections for (n,p), (n,α), (n,f) or (n,γ) reactions.

EXPERIMENTAL

Materials

Gelatine 40 μm thick, backed on a 100 μm thick polyester base (produced by Fotokemika, Zagreb, Yugoslavia), and hydrate cellulose (Elwiphan PT, German Democratic Republic), 30 μm thick, were used as image detection materials.

The response to neutron-induced charged particle was measured by the irradiation of thin samples of boron, gadolinium and uranium which were placed in close contact with the irradiated polymers. For this purpose a 100 μm thick $Li_2B_4O_7$ layer, a 25 μm thick Gd-foil and a 93% enriched uranium fission foil were used.

Carbon steel castings containing 0.01 - 1.5 wt% of boron and UO_2 - Gd_2O_3 pellets containing 0 - 10 wt% of Gd_2O_3 where used to illustrate the applicability of the techniques for imaging of boron in metals and characterization of nuclear fuel, respectively.

Irradiation and Image Processing

All the irradiations in NIA experiments were performed in the core of the TRIGA Mark II reactor at the "J. Stefan" Institute, Ljubljana using aluminium pre ssure type cassettes. The thermal neutron flux was $\sim 4 \times 10^{12}$ $cm^{-2}s^{-1}$ and the gold Cd ratio about 4. For the measurement of response to monoenergetic alpha-particles and protons, the 5 MeV Van de Graaff accelerator of the Institute of Nuclear Research in Debrecen was used. The experimental arrangement is described in an accompyning paper (Somogyi and co-workers, 1983).

A stable relief image was obtained by soaking the irradiated polymer in H_2O for several minutes. For a dyed image, the water contained 0.1 wt% of methylene blue.

The optical density of the dyed image of accelerated ions was measured by a microphotometer at a magnification of 100 and a scanning beam diameter of 5.1 μm. The optical density of neutron-induced autoradiographs was measured by a microphotometer using 2 x 0.02 mm scanning beam. The depth difference between the irradiated and unirradiated region was measured by a TESATRONIC electronic length measuring apparatus.In addition to an optical microscope, a Scanning Electron Microscope (SEM) and Transmission Electron Microscope (TEM) were used for relief image evaluation. In SEM experiments, a 150 Å thick layer of gold was evaporated onto the developed polymer and the picture was taken at an angle of 45°. The operating voltage was 5 kV. For TEM examination, a graphite replica after evaporation at ~ 60° was taken. The operating voltage was 100 kV at a current of 1 A.

RESULTS

Response function

The response of the detector is expressed by two quantities: i) the optical density, D, and ii) the normalized residual thickness, r=(R-t)/R, where t is the thickness of the dissolved material layer and R is the range of the particles.

The optical density vs fluence, Φ_α, of alpha particles (E_α =3.5 MeV) for cellulose hydrate is given in Fig. 1. From this figure it can be seen that first a dyed image is formed at a fluence of about 10^{11} cm^{-2}. The optical density increases with increasing fluence up to 2×10^{12} cm^{-2} which is the threshold value for the formation of a relief image. Due to the dissolution of detector material, the optical density steeply decreases at higher fluences and reaches a stable value at a fluence of about 4×10^{12} cm^{-2} when the removed layer thickness is equal to the range of the alpha particles.

Similar response functions were found for 1.6 MeV protons, $^{10}B(n,\alpha)$ and $^{235}U(n,f)$ reaction products and internal conversion electrons from neutr capture in gadolinium. Examples of observations are given in Figs. 2 and 3 obtained by inter al conversion electrons due to neutron capture in gadolinium and fission fragments, respectivelly. Most of the internal conversion electrons from $^{157}Gd(n,\gamma)$ reaction have an energy of about 70 keV (Harms and McCormack, 1974).

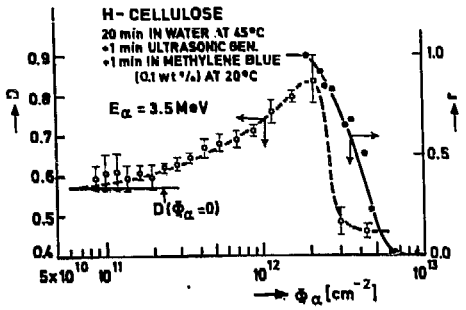

Fig. 1. Optical density, D, and residual foil thickness, r, vs fluence of α-particles, Φ_α.

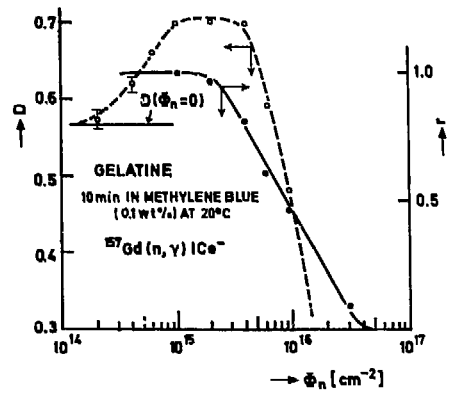

Fig. 2. Optical density, D, and residual foil thickness, r, vs neutron fluence, Φ_n, for gelatine-Gd foil combination

From the results presented in Fig. 3 it can be seen that a high contrast of dyed image can be achieved by heavy ions. Only a few words can be said about the mechanism of the formation of the dyed image. It seems that dyed image formation is a consequence of the preferential diffusion of the dye in the irradiated area because the channels between the broken chain are filled in with the dye after drying.

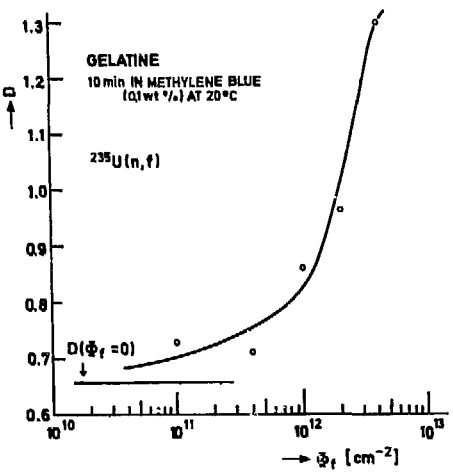

Fig. 3. Optical density, D, vs fluences of fission fragments, Φ_f.

Applications

NIA based on relief and dyed image formation in polymers has potential for applications in several important technological and scientific areas. The nuclear properties of some isotopes which have high cross section for thermal neutron and which could be mapped by these techniques are listed in Table 1.

Table 1 Characteristics of Some Elements which could be Mapped by Thermal Neutron-Induced Autoradiography

Element	Reaction	Abundance %	Cross section (b)	Half life	Energy of charged particles (MeV)
He	$^3_6$He(n,p)$^3_3$H	0.0014	5327	stable	p, 0.578; $^3_3$H, 0.186
Li	^{6}Li(n,α)$^3_7$H	7.7	940	stable	α, 2.05 ; $^3_7$H, 2.74
B	^{10}B (n,α)^{7}Li	19.5	3837	stable	α, 1.48 ; ^{7}Li, 0.84
Rh	^{103}Rh(n,γ)^{104}Rh	100	144	43 s	β$^-$, 2.41 (max)
Ag	^{109}Ag(n,γ)^{110}Ag	48.7	110	24.5 s	β$^-$, 2.87 (max)
In	^{115}In(n,γ)^{116m}In	95.7	154	54 min	β$^-$, 1.0 (max)
Sm	^{152}Sm(n,γ)^{153}Sm	26.6	210	46.7 h	β$^-$, 0.8 (max)
Gd	^{157}Gd(n,γ)^{158}Gd	15.7	240000	stable	ICe$^-$, 0.07 (main)
Dy	^{164}Dy(n,γ)^{165m}Dy	28.1	2000	1.26 min	β$^-$, 1.04 (max)
Au	^{197}Au(n,γ)^{198}Au	100	98.8	2.69 d	β$^-$, 0.962(max)
U	^{235}U(n,f)	0.7	580		

We found that various techniques of contrast enhancement of a relief image can be employed to produce high quality autoradiographs. These techniques are based on: i)dyeing the polymers with organic dye and viewing under transmitted light of an optical microscope, ii) evaporation of opaque substances and viewing under reflected light, iii) illumination under a given angle of incidence and observation of diffuse reflected light, iv) combination of dissolution of irra-

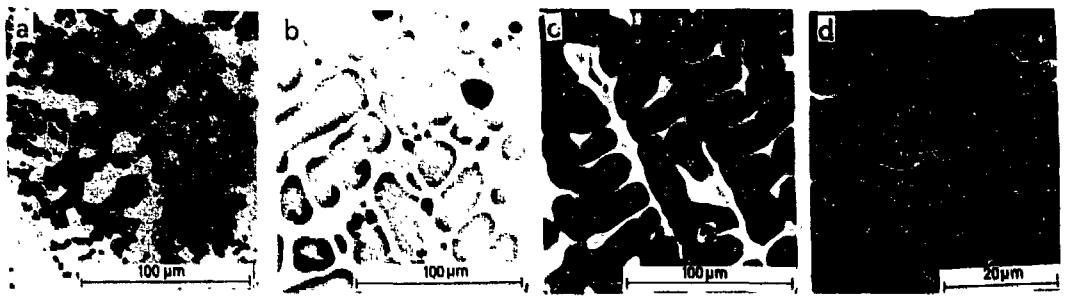

Fig. 4. Neutron-induced boron autoradiograph of steel castings (0.5 wt%B,1 wt%C), a) track-etch method CA-80l5, b) gelatine dyed image, c) gelatine relief image after evaporation of 600 Å thick Al, d) gelatine relief image in combination with SEM.

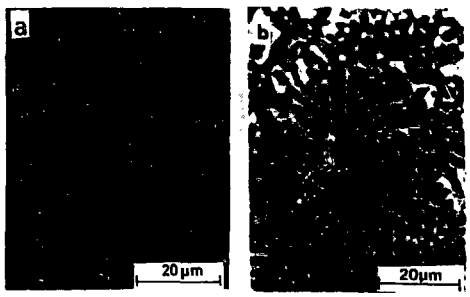

Fig. 5. Microstructure of UO_2-Gd_2O_3 (10 wt%) pellet, a) optical micrograph, b) neutron-induced autoradiograph.

diated gelatine with photographic process using an X-ray film and viewing under reflected light and v) utilization of electron microscopy (SEM and TEM).

Feasibily of the new technique and its superiority over track-etch detectors is illustrated on autoradiographs of boron in steel shown in Fig. 4. Neutron fluence was 3×10^{11} cm^{-2} and 1.4×10^{15} cm^{-2} in the case of track-etch and the new technique respectively. Boron is concentrated in the interdendritic regions of crystal grains, dark areas (Fig. 4a). Small boron free crystals can be clearly observed in the autoradiographs taken with gelatine (Fig. 4b,c,d) due to the high resolving power of this technique.

The applicability of the new technique for the characterization of nuclear fuel is illustrated in Fig. 5, where the microstructure of U_2O_3-Gd_2O_3 nuclear fuel pellet can be seen. White areas in the micrograph (Fig. 5a) correspond to $(U,Gd)O_2$ matrix. Pore structure (dark spots) of a sintered sample can also be seen. A dyed image autoradiograph obtained at neutron fluence of 1.4×10^{15} cm^{-2}, (Fig. 5b), shows that dark areas in Fig. 5a correspond to crystal grains where concentration of uranium is much lower in comparison with $(U, Gd)O_2$ matrix.

CONCLUSIONS

NIA utilizing formation of dyed and/or relief image in polymers was developed. Comparison with techniques based on application of track-etch detectors and X-ray films showed following advantages: i) it is more universal, isotopes which have high cross section for (n,p), (n,α) and (n,f) reactions as well as (n,γ) reactions followed by internal conversion or β-decay can be mapped, ii) it is practically insensitive to γ-rays, iii) it is selective. Response depends on the type and energy of particles and the detector material, iv) it has much better spatial resolution and detail discernment, and v) various techniques can be used to improve image quality. It requires a few orders of magnitude higher neutrons fluences which are, however, easily achievable even in small nuclear reactors. It seems that the new technique is superior.

REFERENCES

Fowler, P.H., and V.M. Clapham, Eds., (1982). Proc. 11th Int.Conf.Solid State Nuclear Track Detectors, Pergamon Press, Oxford.

Harms, A.A., and G. McCormack (1974). Nucl.Instr.Meth., 118, 583-587

Ilić, R., M.Humar, M.Najžer, and A.Podgornik (1980). Proc. 10th Int.Conf.Solid State Nuclear Track Detectors, Pergamon Press, Oxford, pp.689-693.

Najžer, M., M.Humar, and R.Ilić (1982). Proc. 11th Int.Conf.Solid State Nuclear Track Detectors, Pergamon Press, Oxford, pp.77-80.

Somogyi, G., I.Hunyadi, R.Ilić, A.Loose and Zs. Varga (1983). Proc. 12th Int.Conf.Solid State Nuclear Track Detectors, present issue.

Varga, Zs., G.Somogyi, I.Hunyadi, R.Ilić, and A.Loose (1983). Proc. 13th Int.Symp.on Autoradiography, Tabor, in press.

ATOMKI Preprint E/8 (1983)

A NEW POSSIBILITY FOR HIGH-RESOLUTION SPECTROSCOPY OF NUCLEAR PARTICLES ENTERING CR-39 AT SELECTED DIP ANGLES

G. Somogyi*, I. Hunyadi*, A.F. Hafez** and G. Espinosa***

*Institute of Nuclear Research of the Hungarian Academy of Sciences, H-4001 Debrecen, Hungary
**On leave from Alexandria University, Egypt, Present address: Institute of Nuclear Research, H-4001 Debrecen,
***Instituto de Fisica, UNAM, Apartado Postal 20-364 México 20, D. F. México

ABSTRACT

In nuclear reaction studies a differentiation of the reaction products according to their type and energy is generally required. At right angle of incidence a particle identification method based on the relation between the track diameter and particle energy can be well applied to plastic track detectors of low registration sensitivity. We have tried to extend this "track-diameter method" to the high-sensitivity CR-39 sheets by selecting special incident angles for particle detection. The utility of such a measuring procedure, called "track--size method", is presented for alpha and proton spectroscopy. A theory is developed to calculate at arbitrary angles the main parameters affecting the energy resolving power of the "track-size method", namely the critical layer thickness (which has to be removed from the detector surface for track-induction) and the depth and minor axis of etch-pits.

KEYWORDS

Nuclear spectroscopy; CR-39 detector; etch-tracks; etch-pit formation theory; evolution of minor track axis, energy resolution.

INTRODUCTION

Solid-state nuclear track detectors have been increasingly used in numerous fields related to nuclear physics. Extensive work has also been carried out on determining the response characteristics of such detectors as nuclear spectrometers. In nuclear reaction studies an identification of reaction products according to their type and energy is frequently required. For normally incident particles, energy-dispersive track-diameter methods have already become useful scientific tools (Somogyi and Szalay, 1973; Somogyi et al, 1977; Balcázar-Garcia and Cuauhtécatl, 1982; Price, 1982). The method provides sufficiently good, or sometimes excellent resolution, especially for lightly ionizing nuclei.

For alpha-particle spectroscopy, plastic track detectors of low registration sensitivity (e.g. Makrofol-E) have proved to be the most advantageous (Somogyi et al, 1977). We have tried to extend this "track-diameter method" to the high-sensitivity CR-39 as well. Here, however, the usual irradiation geometry with normally incident particles have not resulted in reasonable resolution, even not for protons, but we have obtained excellently high resolution at selected angles of the incoming particles. In this paper, the theoretical background of this extended diameter method, called "track-size" (or minor-axis) method, is considered. We present briefly the basic relations neccessary to predict the most important features of such type of nuclear track spectroscopy. By using the theoretical basis of etch-pit evolution (Somogyi, 1980), a calculation procedure is presented to estimate the resolving power of the new method.

Finally some typical results calculated by the above procedure are shown for two different CR-39 sheets (MA-ND and Homalite) manufactured by the Hungarian Optical Works and the Homalite Ltd. We note that the MA-ND (MOM-ATOMKI Nuclear Detector) is especially produced, high-sensitivity detector.

THEORETICAL CONSIDERATIONS

Critical layer removal (h_c). For a constant $V=V_T/V_B$ etch-rate ratio, the etch-pit evolution can be easily described at any incident angles, only a critical angle given by $\sin\theta_c=1/V$ should be taken into account as a limit angle for track revelation. At varying etch-rate ratio, V(R), along the residual range R, the situation is more complicated (see Fig.1). Here, it is advisable to introduce a so-called critical layer removal, $h_c=x_c\sin\theta$, into the theoretical formalism. The actual value of h_c as a function of the incident angle θ and the "starting range" R_o of the nuclear particles can be easily derived from the solution of the equation:

$$\sin\theta = 1/V(R)\big|_{R=R_o-(h_c/\sin\theta)}. \qquad (1)$$

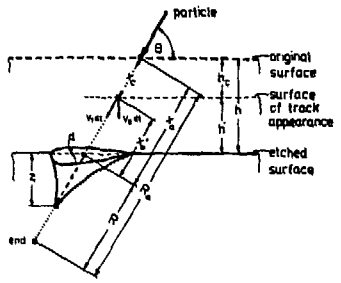

Fig.1. Schematic representation of etch-pit formation, illustrating the meaning of basic quantities used in our calculations.

The V(R) response function for alphas and protons in CR-39 sheets can be well fitted by each of the following equations:

$$V(I)=aR^{-n};\ V^{-1}(II)=1-aR^{-n};\ V(III)=1+aR^{-n}, \qquad (2a,b,c)$$

where a and n are empirical fitting parameters. Substituting the equations (2a,b,c) into equation (1), we have

$$h_c(I)=\sin\theta[R_o-(a.\sin\theta)^{1/n}], \qquad (3a)$$

$$h_c(II)=\sin\theta[R_o-a^{-1/n}(1-\sin\theta)^{1/n}], \qquad (3b)$$

$$h_c(III)=\sin\theta[R_o-(a.\sin\theta)^{1/n}(1-\sin\theta)^{-1/n}]. \qquad (3c)$$

It can be seen that, in practice, two cases are realized: when $h_c=0$ and $h_c\neq0$. In the first case the etch-track formation starts immediately after etching, but in the second case only after certain retardation.

Track depth (z). It is easily seen from Fig.1 that the observable depth of an etch-pit can be given by the following parametric relation:

$$z=x_o\sin\theta-h_c-H_c(x_o);\quad h=h_c+H_c(x_o), \qquad (4a,b)$$

where the validity range of the parameter is $x_c\leq x_o\leq R_o$. From here the maximum possible track depth is obviously

$$z_m=R_o\sin\theta-h_c-H_s;\qquad H=\int_{x_c}^{x}V^{-1}(x)dx, \qquad (5);(6)$$

where $H=H_c(x_o)$ if $x=x_o$ and $H=H_s$ if $x=R_o$, respectively.

Track minor axis (d). Finally, to solve our original task concerning the theoretical foundation of "track-size spectroscopy", we determine the d(h,E) function at selected dip angles for alphas and protons. For the calculation of minor axis, d_c, in the "cone phase" of track formation, we have derived the following parametric relation:

$$(d_c/2)^2=(x_o'\sin\theta-H_c')^2.(V(x_o')\sin\theta+1).(V(x_o')\sin\theta-1)^{-1}, \qquad (7a)$$

$$h=h_c+x_o'\sin\theta+(x_o'\sin\theta-H_c').(V(x_o')\sin\theta-1)^{-1}, \qquad (7b)$$

where $x_o'=x_o-x_c$, $0\leq x_o'\leq R_c-x_c$ and $H_c'=H_c(x_o'+x_c)$. We note here that such formulae, describing the evolution of track minor axis during the first phase of etching, has not been available in the literature.

The minor track axis, d_s, in the "sphere phase" of track formation, can be calculated from the relation

$$(d_s/2)^2=(h-h_c-H_s)^2-(h-R_o\sin\theta)^2. \qquad (8)$$

RESULTS OF CALCULATION

Based on equations (2) - (8), we have developed a computer programme to calculate the variation of the considered characteristic track parameters (h_c,z,d) during etching and the resolving power ($\Delta d/\Delta E$) of the "track-size method" proposed. Our aim here is to demonstrate some typical results obtained for several realistic cases by our computation programme.

A basic requirement for the performance of the above-mentioned calculations

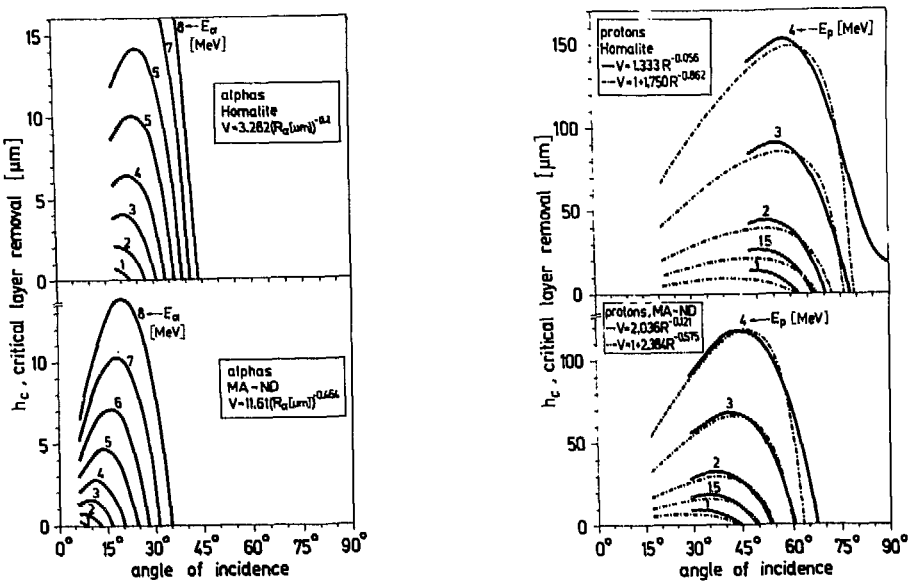

Fig.2. Dependence of the critical layer removal on the incident angle of alphas and protons in MA-ND and Homalite CR-39 sheets.

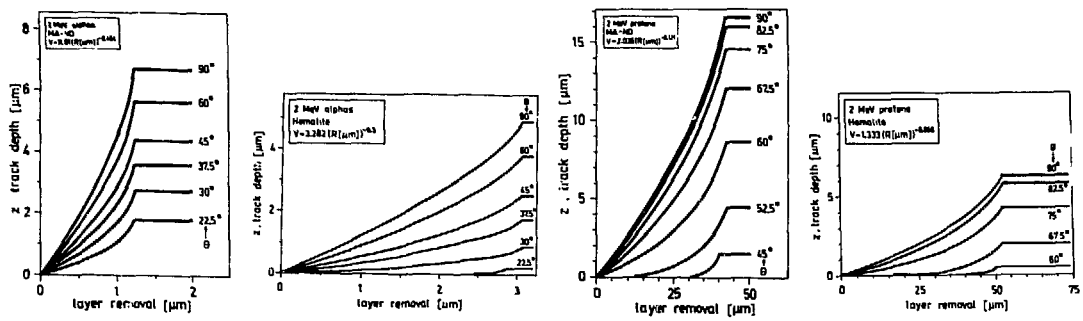

Fig.3. Calculated curves showing the dependence of observable track depth on the layer removal for alphas and protons in MA-ND and Homalite CR-39.

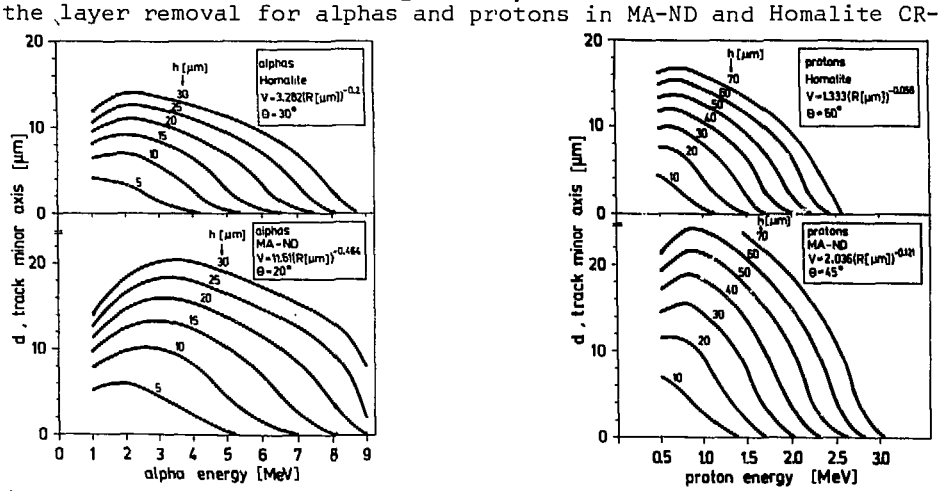

Fig.4. Calculated curves showing the dependence of track minor axis on the alpha and proton energy in MA-ND and Homalite CR-39 sheets.

is the knowledge of the response function $V(x_0')$. In addition, it is expedient to choose its form so that the integral H, given by equation (6), be explicitly calculable. In our calculations we used the simple power function defined by equation (2a), i.e. the form $V(x_0') = a(R_0-x_0'-x_c)^{-n}$, where a and n were determined experimentally for both MA-ND and Homalite CR-39 sheets and their values are indicated in each figures. It should be mentioned that the form (2c) gives the best fit to the measured response, by using this, however, a numerical integration of H is required. Finally, the range-energy relations for alphas and protons were taken from a table published by Almási and Somogyi (1981).

First, we illustrate the variation of $h_c(\theta)$ function calculated by equation (3a) for alphas and protons registered in two CR-39 sheets of different sensitivity. The calculated curves shown in Fig.2 indicate a surprisingly large effect of retardation in the first track appearance in a given interval of incident angles. Actually, this very energy dependent effect stimulated us to develop the high-resolution nuclear track spectroscopy presented here.

We would like to emphasize that the $t_c=h_c/V_B$ delay time in track formation results merely from the "track-etch kinetics" and it has nothing in common with the "registration threshold" or "etch-induction time". Unfortunately, however, in some recent reports these quantities of quite different physical content are not clearly distinguished, which may result in misinterpretation of certain etching effects in CR-39.

If the condition $h \geq h_c$ is satisfied, both the depth and surface opening of tracks start to grow. Both z and d should have simultaneously higher value than a limit to be observable under optical microscope (e.g. 0.5 μm). Taking this into consideration, we can use our calculations to estimate the registration efficiency of CR-39 under various track registration and etching conditions.

The typical trend of the variation of $z(h)_\theta$ function calculated by equation (4) is presented in Fig.3. At those angles where $h_c=0$, the formation time of the maximum track depth is identical.

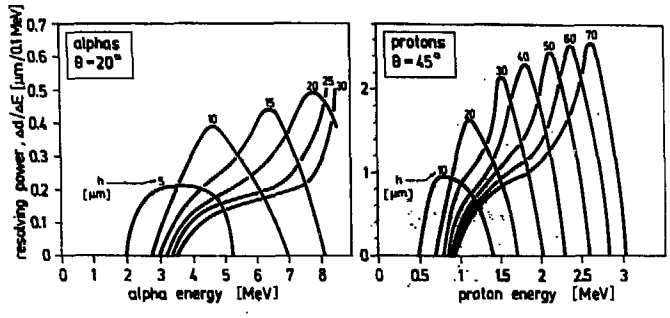

Fig.5. Calculated curves showing the resolving power of the "track-size method" for alpha and proton spectrometry in MA-ND CR-39 sheet at specially selected incident angle.

For nuclear track spectroscopy the most important information is involved in the $d(E)_h$ curves shown in Fig.4. From the slope of these curves at different energies, we can derive the relation $\Delta d/\Delta E=f(E)_h$ (see Fig.5) which represents the resolving power of the proposed spectroscopical method based on the high sensitivity of the minor track axis to the variation of particles energy at specially selected angles.

REFERENCES

Almási, Gy., and G. Somogyi (1981). Range and REL data for light and heavy ions in CR-39, CN-85 and PC nuclear track detectors. ATOMKI Közl. 23, 99-112.

Balcázar-Garcia, M., and V. Cuauhtécatl (1982). A method to determine the energy per nucleon of isotopic beams utilizing SSNTDs. Proc. 11th. Int. Conf. Solid State Nuclear Track Detectors, Bristol, Pergamon Press, 283-286.

Price, P.B., (1982). Application of plastic track detectors to atomic, nuclear, particle, and cosmic ray physics. Proc. 11th. Int. Conf. Solid State Nuclear Track Detectors, Bristol, Pergamon Press, 737-750.

Somogyi, G., and S.A. Szalay (1973). Track-diameter kinetics in dielectric track detectors. Nucl. Instrum. Meth. 109, 211-232.

Somogyi, G., I. Hunyadi, E. Koltay, and L. Zolnai (1977). On the detection of low-energy He-4, C-12, N-14 and O-16 ions in PC foils and its use in nuclear reaction measurements. Nucl. Instrum. Meth. 147, 287-295.

Somogyi, G. (1980). Development of etched nuclear tracks. Nucl. Instrum. Meth. 173, 21-42.

ATOMKI Preprint E/9 (1983)

EFFECT OF PARTICLE FLUENCE ON TRACK DIAMETER AND RESPONSE OF ELECTROCHEMICALLY ETCHED SSNTD

K. Turek[x] and G. Dajkó[xx]

x Institute of Radiation Dosimetry of the Czechoslovak Academy of Sciences, 180 86 Prague, Czechoslovakia
xx Institute of Nuclear Research, 4001 Debrecen, Hungary

ABSTRACT

Track diameter as a function of particle fluence is given for electrochemically etched fission fragment tracks. It is shown that high particle fluences decrease the developability of electrochemically etched tracks. Therefore the dependence of sensitivity on particle fluence was studied for polyester and poly(allyl diglycol carbonate). Continuously decreasing sensitivity was found even in the case when track overlap does not occur. An idea for correct interpretation of the response is suggested.

KEYWORDS

Melinex-O, CR-39, fission fragment, neutron, electrochemical track etching, particle fluence, mutual effect, track diameter, sensitivity, energy dependence.

INTRODUCTION

The electrochemical etching technique, ECET, is very useful method of processing plastic SSNTDs (Tommasino, 1970). It makes the track evaluation easier and less tedious. Very high gradient of electric field strength is created at the tip of tracks and it leads to the formation of large and contrasty discharge spots (henceforth referred to as E-tracks).

It follows from the principle of ECE and it has also been proved (Tommasino, 1977; Al-Najjar et al., 1979) that individual tracks can interact mutually by their electric fields. In this work, we have tried to study in details practical aspects of this "track interaction". We have paid special attention to the dependence of the diameter of E-tracks on the fluence of fission fragments and to that of the sensitivity of detectors on the neutron fluence when using no fissionable radiator.

EXPERIMENTAL CONDITIONS

PET foils (Melinex-O, 100 μm) and CR-39 (Pershore, 300 μm and 650 μm) plastic sheets were used. These three detectors will be referred to as PET, CR-39(I), CR-39(II). Irradiation by fission fragments (perpendicularly to the detector surface) was carried out using ^{252}Cf source in a vacuum chamber. As concern the neutron sources used see Table 1. Samples were fixed perpendicularly to the beam axis. CR-39 sheets were covered by 2 mm thick polyethylene during irradiation.

For the ECET a vessel with arrangement similar to that described formerly by Al-Najjar et al. (1978) was used. Electrochemical etching was carried out only on the detector surface faced towards the source (1 mol KCl solution was used from opposite side). A power supply of sinusoidal pulses was used. The field strength was given by the amplitude of applied pulses divided by the initial foil thickness. Sheets of CR-39 were etched by the combined

TABLE 1 Neutron sources used for this study

Neutron source	Reaction	Energy, resp. mean energy (MeV)	Neutron fluence monitoring	Institute
Generator NA-2	$^{3}H(d,n)$	14.7	recoil proton telescope	Inst. of Radiation Dosimetry, Prague, Czechoslovakia
Am-Be	$^{9}Be(\alpha,n)$	4.4	calculation	
^{252}Cf	fission	2.1	"	
Van-de-Graaff accelerator	$^{3}H(p,n)$	0.57	TE-ionization chamber, GM-counter, long counter (de Pangher), BF_3-counter in moderating sphere	Inst. für Strahlenschutz, Neuherberg, F.R.G.
	$^{3}H(p,n)$	1.9 - 2.1		
	$^{2}H(d,n)$	5 - 5.5		
	$^{3}H(d,n)$	15 -15.3		
Cyclotrone U-120	$^{9}Be(d,n)$	6.2	deutoron charge integrator	Zentralinstitut für Kernforschung, Rossendorf, G.D.R.
	" + 10cm Fe	3.1		
	"+10 cm paraf.	4.2		
Generator SAMES	$^{2}H(d,n)$	3.3	long counter (de Pangher)	CEN Fontenay-aux-Roses, France
Reactor SILENE	fission	0.3	activ.spectrometer SNAC	CEN Valduc, France
Tandom generator	$^{3}H(p,n)$	1 2.5	long counter (de Pangher)	LLNL Livermore, U.S.A.

technique described by Somogyi et al. (1981). E-tracks were measured and counted by a projection microscope. The background track density was substracted from the measured values.

RESULTS AND DISCUSSION

PET-foils irradiated by fission fragments of fluences between $7x10^3$ and $9x10^5$ cm^{-2} were electrochemically etched. The diameters of E-tracks decreased with increasing fluence as shown in Fig.1 and this decrease is more pronounced for longer etching times. It is obvious, that at small E-track diameter (short conductive treeing-branches) the interaction among the electric fields of individual tracks is substantially reduced.

At present stage, we suppose that the principle of the mutual effect is the same as proposed by Al-Najjar et al. (1979), i.e. antiparallel components of electric field strength jam each other.

Several additional experiments were carried out to prove that the mentioned mutual effect can affect the sensitivity. For PET detectors we have found that for both perpendicular incidence and 2π -geometry the sensitivity (E-tracks per fission fragment) remains independent on the fission fragment fluence until the overlapping of E-tracks occurs.

Our following task was to study the behaviour of sensitivity (E-tracks per neutron) in case of neutron-induced recoil tracks. In comparison with fission tracks recoil tracks produced by the commonly used neutron sources are less favourable for creation E-tracks (shorter etchable track length, smaller ratio V_t/V_b). We have supposed that the influence of mutual effect on the sensitivity of electrochemically etched SSNTDs should be more profound in the case of neutron-induced recoils. Some results published by Al-Najjar et al. (1979) indicated this possibility. To prove it, the neutron fluence was changed to cover at least the range of one order. The measured values of sensitivity are plotted in Figs. 2 and 3 (Turek, 1982). Dashed strips on these figures correspond to background density region and dashed lines with indicated number are so-called "isodensitic lines"(connecting points of constant value of product "sensitivity x fluence = = E-track density"). Dot-and-dash lines correspond to constant neutron fluences. Regardeless on the kind of detector and neutron energy, it is obvious that sensitivity to neutrons continuously decreases even in the E-tracks density region where overlapping cannot have practical importance (in our case it starts to appear at E-tracks density of about $4x10^3$ cm^{-2}).

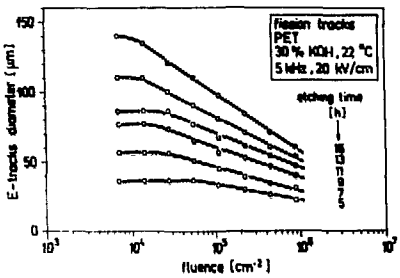

Fig.1. Diameter of fission fragment E-tracks in PET as a function of fluence for different etching times

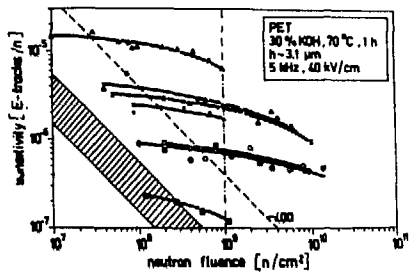

Fig.2. Sensitivity of PET to neutrons as a function of the neutron fluence: Δ -14.7 MeV, ▲ -Am-Be, X - ^{9}Be(d,n)+10cm Fe, + -3.3 MeV, O - 5.25 MeV, ● - ^{252}Cf, ■ -react.Si

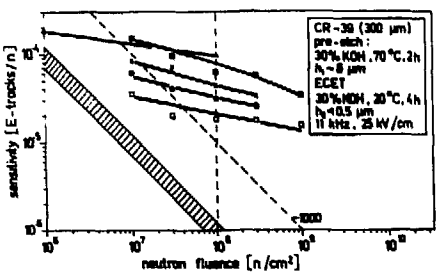

Fig.3. Sensitivity of CR-39(I) to neutrons as a function of the neutron fluence: □ -0.57 MeV, ■ -1.9 MeV, Δ -3.3 MeV, X -5.25 MeV, ● -15.1 MeV

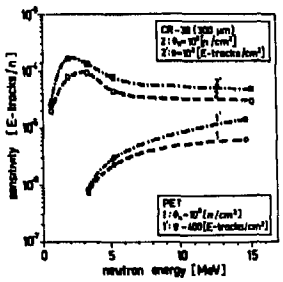

Fig.4. Estimated energy dependencies at given values of parameters (inter- or extrapolated from Figs.2,3)

In spite of shortage of detailed knowledge regarding the mechanism of mutual effect among E-tracks, it seems that sensitivities can differ substantially depending on neutron fluence at which they are determined. This observation leads to the question how to determine correctly energy dependence of electrochemically etched detectors.

One way is to compare sensitivities obtained at the same neutron fluence (i.e. points lying on dot-and-dash lines in Figs.2 and 3). However, such sensitivities correspond to different E-tracks densities with respect to neutron energy; therefore the "intensity" of mutual effect is different for each energy. At the same neutron fluence more E-tracks is created for that energy to which the given detector is more sensitive. As a consequence of the higher E-tracks density the mutual effect is higher too. However, due to higher mutual effect, some "poor" tracks (shorter etchable track length, low V_t/V_b value, unfavourable angle of incidence) cannot be developed as E-tracks in spite of their developability in less critical case (lower E-tracks density).

The comparison of sensitivities obtained at the same E-tracks density (i.e. points on proper isodensitic line) seems to be more correct. In this case we may suppose that the mutual effect is of the same level for any neutron energy as well as the degree of degradation of E-tracks formation. In Fig.4 the estimated dashed and dot-and-dash lines serve more or less to joint corresponding points; because of lack of experimental data such curves fit only roughly the exact energy dependencies for both PET and CR-39(I) detectors. The indicated points were interpolated or extrapolated from Figs. 2 and 3. It is obvious that the shape of curves is influenced by the method of the choice of sensitivity values (either at the same fluence or at the same E-tracks density).

From the obtained results one can draw two conclusion for correct fitting of the energy dependence of SSNTDs treated by ECET:

a/ Values of sensitivity used for fitting should be related either to constant neutron fluence or to constant E-tracks density as a parameter. First possibility is experimentally easily achievable, however, the latter one seems to be more correct, because variability of the mutual effect at different E-tracks density is eliminated.

b/ Energy dependence of electrochemically etched SSNTDs should be taken into account absolutely only for a given value of choosen reference parameter (neutron fluence or E-tracks density). For correct comparison of results obtained by ECET, the value of corresponding parameter should be added to the description of etching conditions.

As a general conclusion, it is necessary to point out that mutual effect among E-tracks cannot be omitted and it should be carefully taken into account for correct interpretation of the results.

REFERENCES

Al-Najjar S.A.R., Balcázar-Garcia M. and Durrani S.A. (1978). A multi-detector electrochemical etching and automatic scanning system. Nucl. Tracks, 2, pp. 215-220.

Al-Najjar, S.A.R., Bull R.K. and Durrani S.A. (1979) Electrochemical etching of CR-39 plastic: application to radiation dosimetry. Nucl. Tracks. 3. pp. 169-183.

Somogyi G., Dajkó G., Turek K. and Spurny F. (1981) Characteristics of neutron-irradiated CR-39 foils treated by sequential chemical and electrochemical etching. Proc.11th Int. Conf. on SSNTDs, Bristol, 1982, pp. 445-449.

Tommasino L. (1970) Electrochemical etching of damaged track detectors by H.V. pulse and sinusoidal waveform. Int. Report RT/PROT.1. Lab. Dosimetria e Standardizzazione CNEN, Casaccia, Roma, Italy

Tommasino L. (1977) Electrochemical etching for personnel neutron dosimetry. 6th ERDA Workshop on Pers. Neutr. Dosimetry, PNL-2449/UC-48, Pacific Northwestern Laboratory, Richland, Washington, pp. 101-104.

Turek K. (1982) Study of polymer SSNTDs for application in neutron detection and dosimetry. Thesis (in Czech.), Faculty of Nucl. Sci. and Phys. Engineering, Czech Technical Univ., Prague

ATOMKI Preprint E/10 (1983)

DEVELOPMENT OF A CCD BASED SYSTEM CALLED DIGITRACK FOR AUTOMATIC TRACK COUNTING AND EVALUATION

J. Molnár, G. Somogyi, S. Szilágyi, and K. Sepsy

Institute of Nuclear Research of the Hungarian Academy of Sciences, H-4001 Debrecen Hungary

ABSTRACT

Rather expensive and unflexible commercial systems have been reported in the literature for fully automatic counting and analyzing etched nuclear tracks. In these systems the image processing is made by a videocamera equipped with a microscope of relatively high magnification. We have developed, to best of our knowledges, the first automatic track analysis system (DIGITRACK) in which the video signals are processed by a new type of videoreceiver called charged coupled device (CCD). The photosensitive semiconductor device is a 2.5 cm long line imager of type Fairchild CCD 121HC which converts one row of the picture seen through a low magnification microscope into 1728 binary signals by a thresholding logic. The picture elements are analysed by a microcomputer equipped with two INTEL 8080 microprocessors and interfaced to a PDP-11/40 computer. The microcomputer also controls the motion of the stage of microscope. For pattern recognition and analysis a software procedure is developed which is able to differentiate between overlapping tracks and to determine the number, surface opening and x-y coordinates of the tracks occurring in a given detector area. The distribution of track densities and spot areas on the detector surface can be visualized on a graphic display. The DIGITRACK system has been tested for analysis of alpha-tracks registered in CR-39 and LR-115 detectors.

KEYWORDS

CCD videoreceiver; microprocessor control; digital image; automation; nuclear track counting; track overlap.

INTRODUCTION

A microprocessor-supported instrument, called DIGITRACK, equipped with a CCD videoreceiver, is developed for automatic evaluation of etched tracks in solid state nuclear track detectors.

We apply such detectors to several practical problems, e.g. to sub-surface uranium prospection and environmental radioactivity measurements. Related methodical and field researches require the evaluation of a large quantity of α-sensitive track detectors. The performance of these tasks is successfully possible only with a microprocessor-supported, versatile image analysing system. When this demand in our laboratory was formulated (in 1977), such an equipment for analysing solid-state nuclear track detectors was not available. Though comparable image-analysing systems (e.g. Quantimet; Magiscan), usable for similar tasks, existed for several reasons weren't suitable for our purposes. Such videocamera-based image analysing systems, even connected with greater computers, are relatively slow, as they are able to identify nuclear tracks only at large magnifications (Schott et al., 1977; Azimi-Garakani and Williams, 1977; Beer et al, 1982).

Accordingly we have decided the development of a new type of nuclear track evaluation system based on a novel light-sensitive solid state device,

the so-called CCD (Beynon, 1980). The task to be solved was also much helped by the disposal of the excellent track contrast-providing α-sensitive track detector of CR-39. Using this detector we could eliminate more easily the background effects too. At the same time, the high spatial resolution of the CCD (with a light-sensitive cell of area 13x17 μm^2) made the use of lower microscope magnifications (2-10x) possible. Thus the speed of track evaluation could be increased.

HARDWARE SYSTEM

The automatic evaluation of solid state nuclear detectors basically means the solution of the following tasks: counting of tracks, measurement of track features (x-y coordinates, track axes, area), record and evaluation of measured track data.

A schematic block diagram of the DIGITRACK system developed by us for the above purposes is presented in Fig. 1, its photograph is shown in Fig.2.

Main processor unit (μP1). The tasks to be performed by the main microprocessor unit are as follows:

- keeping contact with the user via an alphanumeric display and an ASCII keyboard (setting the measuring parameters, information on the detector, value of detector area to be scanned, speed of microscope stage, etc; giving the required way of evaluation: track counting, spatial distribution of track density, track area distribution),
- evaluating track configurations (single, double) received continuously from the image processor unit, determination of various track parameters,
- displaying and recording the results of track evaluation via peripheral units.

The microcomputer used by us is based on an INTEL 8080 type microprocessor. Its construction is modular. Besides its basic configuration it contains the following units:

- serial communication unit[INTEL 8251]towards a PDP 11/40 computer,
- parallel link to the image processor unit[INTEL 8255],
- dual-image graphic display of 256x256 resolution provided with self-refreshing controller,
- alphanumeric video-terminal with self-refreshing interface,
- X-Y plotter interface,
- SEIKO 101F printer interface.

We note that the flexibility of the DIGITRACK instrument and the possibility of its further development, depends on the design of main processor unit. As the need of users frequently claims the use of the system both for special track analyses and large-scale track counting, the instrument is linked to a PDP 11/40 central computer too. In this way an improvement of the hardware/software features of the system is achieved. In this sense, the automatic analysing system of nuclear tracks became an intelligent terminal of a central computer.

Image process unit (μP2). The main tasks of the image processor unit are as follows:

- to control the motion of microscope stage during image analysis,
- to collect bit patterns arriving continuously from the CCD,
- to recognize bits associated with the area of single tracks and to send the separated track images to the main processor.

The μP2 microcomputer in basic configuration is the same as the μP1. Its special units are the following:

- clock generator and driver which provides the control signals for the CCD,
- CCD memories M1, M2, M3 which store, by direct memory addressing (DMA), 3x8 rows of the digitized image,
- stage-driving motor controller and coordinate decoder which ensure the motion of track detector during image analysis.

The track picture is viewed by a Leitz Ortholux research microscope. In addition to this a CCD videoreceiver, a position coder of type Heidenhein and an electromechanical driving system is mounted.

The photoelectric converter in the videoreceiver is a semiconductor device of type Fairchild CCD 121 HC, that converts one row of the picture to be analysed into 1728 binary signals. These are provided in one video-signal.

This video-signal is processed by a thresholding logic which converts it into two gray-levels (0 and 1) (Fig.3).

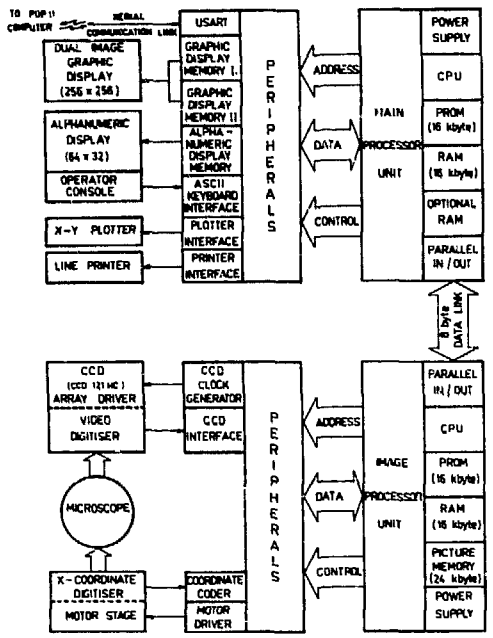

Fig. 1. Block diagram of the DIGITRACK system developed for automatic evaluation of plastic track detectors.

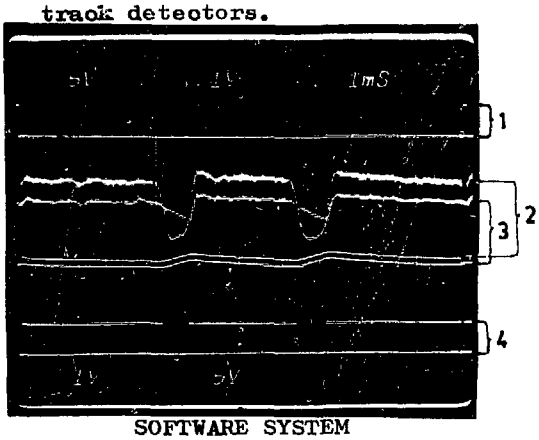

Fig. 3. Digitized image of two alpha tracks in CR-39 detector, displayed on a TV screen.
1. impulses identifying one CCD row,
2. videosignal of one CCD row,
3. output signal of the comparator,
4. digitized video-signal including two tracks.

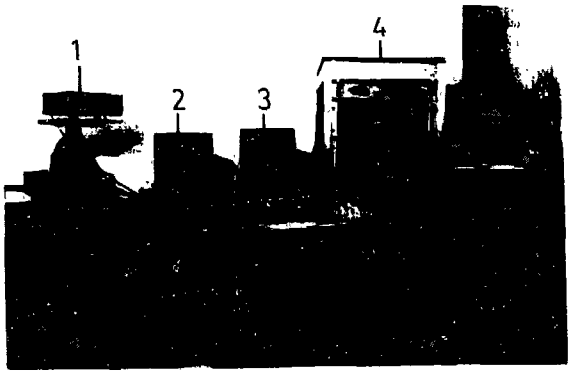

Fig. 2. Photograph of the DIGITRACK system:
1. Box containing the CCD video-receiver mounted on a Leitz-Ortolux microscope,
2. Alphanumeric display terminal,
3. Dual-image graphic display,
4. Micro-computer unit,
5. X-Y plotter,
6. Line printer.

SOFTWARE SYSTEM

The DIGITRACK system itself is devoted mainly to the evaluation of solid state nuclear track detectors. The system can also work as an intelligent terminal of a PDP 11/40 computer, with an additional monitor programme that contains:

- monitor commands for further programme development in both microprocessors,
- communication link between the two microprocessors via a parallel asynchronous line,
- communication link between the PDP 11/40 and the microprocessors via a serial line.

The software tasks are split among the two μP-s in accordance with the hardware. The evaluation of a given track detector by the DIGITRACK system can be performed in the following way: After setting and focusing the nuclear track detector under the microscope, the user gives, via an ASCII keyboard, the programme start conditions (e.g. optical magnification, detector-identifying notes, motor speed, operating mode, parameters of the digitized track image display and data record). Based on these start conditions, μP1 sets and initiates that part of the program which is situated in μP2. Then, the stage driving motor starts and the data collection and image processing begin. In μP2 there are three CCD-memories (M1, M2, M3) at our disposal for the collection of digitized bit patterns arriving from the CCD. Each of them can store 8 rows of CCD information.

Because of the continuous detector motion, a synchronisation between data collection and image evaluation is needed. The program starts after filling the first 16 CCD rows in the memories M1 and M2. By the time M3 is filled with further 8 CCD rows, M1 is evaluated. Then M1 is filled and M2 is evaluated, and that is followed by the filling of M2 and evaluation of M3. This cyclic data collection and evaluation lasts till the wanted statistical accuracy (e.g. given track number or detector area) is satisfied.

During the evaluation of one CCD-memory, μP2 seeks for continuous track images that start in this memory and are continued, perhaps, in the next one. After finding a continuation of the image, μP2 sends it to μP1 and seeks for another image. The μP1 analyses the received track images and, in accordance with the given operating mode, determines the position and area of tracks and separates the overlapping tracks. On the previously displayed track image, one can visually control the discovered and evaluated tracks. Thus track search in μP2 and evaluation in μP1 run parallel. If μP2 has finished with the actual CCD memory, waits until the memory is filled with further 8 rows of data, and the programme goes on with the evaluation of the next CCD memory content. When the desired statistical accuracy is achieved, data collection stops, the motor moves the stage of microscope in its start position and stops. The μP1 displays on the alphanumeric display and on the dual-image graphic display all the data concerning the evaluated tracks. For the preservation of data, the display information is drawable on a plotter and the text information on a printer. Meanwhile, the next detector sheet can be prepared for evaluation.

CONCLUSION

The DIGITRACK instrument in performance of the hardware and software is more-or-less analogous to the commercially available image analysing systems. Here, however, the automatic image analysis is performed by a new type of videoreceiver, a photosensitive semiconductor device called CCD. The use of large-scale integrated circuits and microprocessors has made it possible to build up a rather cheap instrument for evaluation of coordinates, areas and spatial densities of etched nuclear tracks and their statistical distributions.

ACKNOWLEDGEMENT

The authors are grateful to J. Koch and his coworkers at the Central Research Institute for Physics for the collaboration and fruitful discussions in the development of CCD electronic circuits.

REFERENCES

Azimi-Garakani, D., and J.G. Williams (1977). Automatic fission track counting using the Quantimet 720. Nucl. Instr. Meth. 147, 69-73.

Beer, J., J. Pipper, and W. Heinrich (1982). Automatic measurements of nuclear track in plastic foils. J. Phys. E: Sci. Instrum. 15, 439-443.

Beynon, J.D.E., (1980). Charge-coupled devices: concepts, technology and limitations. The Radio and Electronic Engineer. 50, 201-204.

Schott, J.U., E. Schopper, and R.Staudte (1977). A high precision video--electronic measuring system for use with solid state track detectors. Nucl. Instr. Meth. 147, 63-67.

ATOMKI Preprint E/11 (1983)

STUDY OF ^{210}Pb AND ^{210}Po DISTRIBUTIONS IN ENVIRONMENTAL SAMPLES BY CR-39 TRACK DETECTOR

I. Hunyadi, G. Somogyi and S. Szilágyi

Institute of Nuclear Research of the Hungarian Academy of Sciences, H-4001 Debrecen, Hungary

ABSTRACT

Activity concentration distributions of long-lived alpha-emitters in aerosol samples are analysed by high-resolution autoradiography in CR-39. A study of the alpha-activity attached to aerosols of different particulate sizes separated by a cascade impactor is also performed. It is found that, in the majority of samples, the alpha-activity can be dominantly related to the presence of ^{210}Po produced by its beta-active precursor ^{210}Pb. In our studies we have applied the following methods: 1) analysis of alpha-decay properties by means of autoradiographs taken at different post-sampling times, 2) spectroscopical study of individual alpha-tracks and track clusters by a method developed by us for high-resolution alpha-energy determination. In the second method the parameters to be measured are the major axis of surface track opening, the diameter of etched out track end, the total length measurable on the surface along the projected track, and the thickness of layer etched away from the detector surface.

KEYWORDS

Nuclear analytical methods; CR-39 track detector; autoradiography; environmental alpha-activity; aerosols; ^{210}Pb and ^{210}Po distribution, alpha-energy spectroscopy.

INTRODUCTION

Recently the analytical applications of the method of nuclear track detection in dielectric solids are rapidly increasing. Beside the conventional analytical procedures, the etch-track technique has proved to be the most powerful complementary or, in many cases, the only economically applicable alternative to determine concentrations, spatial distributions and seasonal variations of alpha-active nuclides in environmental samples, or in the environment itself. In this way, for low-level alpha-activity measurements, the complex radiochemical procedures and radiation detectors equipped with electronic analysis systems can be replaced by much more simple and easily portable track measuring devices.

The unique registration sensitivity of CR-39 nuclear track detector to high-energy alpha-particles opens several new fields in autoradiographic applications. In addition to the capability for registration of even very low level of environmental alpha-activities in long-term measurements, the CR-39 provides possibility for spectroscopical identification of various α-radioactive elements, too.

We have introduced the nuclear track method to the analysis of long-lived alpha emitters in ground-level air samples. The main sources of these radioactive nuclides in the atmosphere are the ^{222}Rn (radon) and ^{220}Rn (thoron) emanating from the ground. The radon decays in a relatively short time into a long-lived (22.3y half-life) beta-active lead isotope (^{210}Pb) while the thoron into a stabile one (^{208}Pb). The charged decay products are immediately captured by aerosols then, after a given mean residence time (about one week) in the atmosphere, are deposited back to the soil surface. In this way it is apparent that everything in the environment (atmosphere, lands, waters, plants, animals and population) is more or less "contaminated" by ^{210}Pb and its alpha-active decay product ^{210}Po. The study of their concentration distributions is of

considerable importance as they dominantly contribute to the natural radiation burden of population. In addition, they are very suitable tracers to various geophysical, meteorological, biological and other processes in the nature.

The methods used in our present work for studying environmental ^{210}Pb and ^{210}Po activity concentrations in aerosol samples are as follows: i) Analysis of alpha-decay properties by high-resolution and high-efficiency autoradiography taken in CR-39 at different times after collecting the samples. ii) Determination of ^{210}Pb and ^{210}Po activities attached to aerosols collected from air and the variation of these activities with the size of particulates separated by a cascade impactor. iii) Analysis of the energy spectrum of alpha-particles originating from aerosols by measuring suitable geometrical parameters of etched tracks in CR-39 autoradiographs. To the latter task we have developed a calculation method and programme which is analogous but not identical, to the high-resolution spectroscopical method proposed by Fews and Henshaw (1982).

DETERMINATION OF ^{210}Pb AND ^{210}Po FROM DECAY AND BUILD-UP CURVES

The activity concentration of both ^{210}Pb and ^{210}Po can be simultaneously determined from the analysis of curves describing the radioactive decay and build-up if mostly long-lived radon daughters are present in the sample to be studied. According to the radioactive decay series:

$$^{210}\mathrm{Pb}(22.3\mathrm{y}) \xrightarrow{\beta} {}^{210}\mathrm{Bi}(5\mathrm{d}) \xrightarrow{\beta} {}^{210}\mathrm{Po}(138.4\mathrm{d}) \xrightarrow{\alpha} {}^{206}\mathrm{Pb}(\mathrm{stable})$$

^{210}Po is the last radioactive product in the chain, and its 5.3 MeV alpha-particle energy is very suitable for radiographic studies with CR-39 track detector. In an environmental sample, the overall alpha-activity concentration due to polonium, $A_t(\Sigma Po)$, measurable at a $\underline{t}$ time elapsed after sampling (henceforth post-sampling time), is build up from the following three decay chains fed by ^{210}Po, ^{210}Bi and ^{210}Pb of initial concentration $A_o(Po)$, $A_o(Bi)$ and $A_o(Pb)$:

$$^{210}\mathrm{Po} \rightarrow A_t^{Po}(Po); \quad {}^{210}\mathrm{Bi} \rightarrow {}^{210}\mathrm{Po} \rightarrow A_t^{Bi}(Po); \quad {}^{210}\mathrm{Pb} \rightarrow {}^{210}\mathrm{Bi} \rightarrow {}^{210}\mathrm{Po} \rightarrow A_t^{Pb}(Po).$$

Taking these into account, the expectable overall alpha-activity concentration in a sample at $\underline{t}$ post-sampling time will be

$$A_t(\Sigma Po) = A_t^{Po}(Po) + A_t^{Bi}(Po) + A_t^{Pb}(Po).$$

An explicite formula describing the variation of $A_t(\Sigma Po)$ as a function of the time after sampling is given in Fig.1. This equation is derived from the solution of the well-known differential equations applied for the above-mentioned radioactive decay processes. We note that details concerning this calculation can be found in the paper by Winkler et al (1981), who reported a direct alpha-spectrometric method using ionisation chamber to measure activity concentrations of airborne ^{210}Pb and ^{210}Po at two post-sampling times. In Fig.1 we have illustrated the shape of decay and build-up curves at different initial ^{210}Po concentrations. Such curves are directly applicable to the evaluation of ^{210}Pb and ^{210}Po activity concentrations. For the initial concentration ratio $A_o(Bi)/A_o(Pb)$ a value of 0.4 was used in agreement with that derived from the mean residence time of aerosols in normal surface air. In fact, however, as Winkler and others (1981) have shown, the results of these calculations are not very dependent on the actual value of the above ratio. In addition, in practical calculations, the second term in the equation given in Fig. 1 can be neglected.

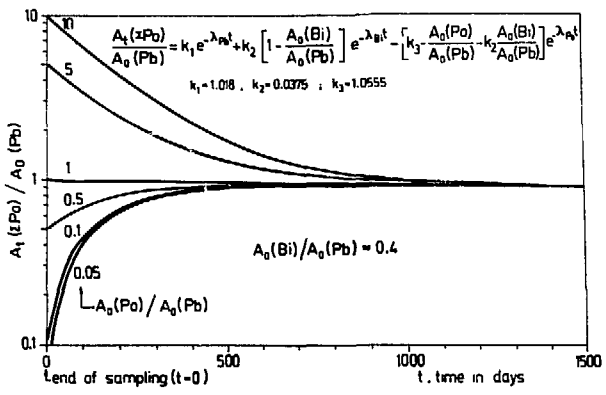

Fig.1. Normalized overall ^{210}Pb activity concentration as a function of post-sampling time. The parameters indicate the ratio of the initial ^{210}Po and ^{210}Pb activities.

A typical evaluation procedure requires the preparation of three autoradiographs with CR-39 in contant with the environmental sample, using about 8-10 week exposures at properly chosen post-sampling times. It is advisable to make the third autoradiograph about one year after sampling, when both the second and third term in the equation in Fig. 1 can be neglected, and A_o(Pb) can be directly obtained only from this last measurement with considerable accuracy. Thereafter A_o(Po) can be derived independently from each of the first two alpha-activity measurements. In addition, these two measurements provide data on the precision of the evaluation method, as well.

DETERMINATION OF ALPHA-ENERGY SPECTRUM FROM TRACK PARAMETERS

Alpha-emitting nuclides can be identified by analysing the geometrical parameters of individual etch-pits in α-autoradiograms taken by CR-39 track detector. This method is based on the determination of range (energy) spectrum of α-particles from proper etch-track parameters. The possibility of the application of such a measuring procedure to high-resolution α-particle spectroscopy was first proposed by Fews and Henshaw (1982) and applied to the study of micro-distribution of α-active nuclei in human lung (Henshaw and Fews, 1982).

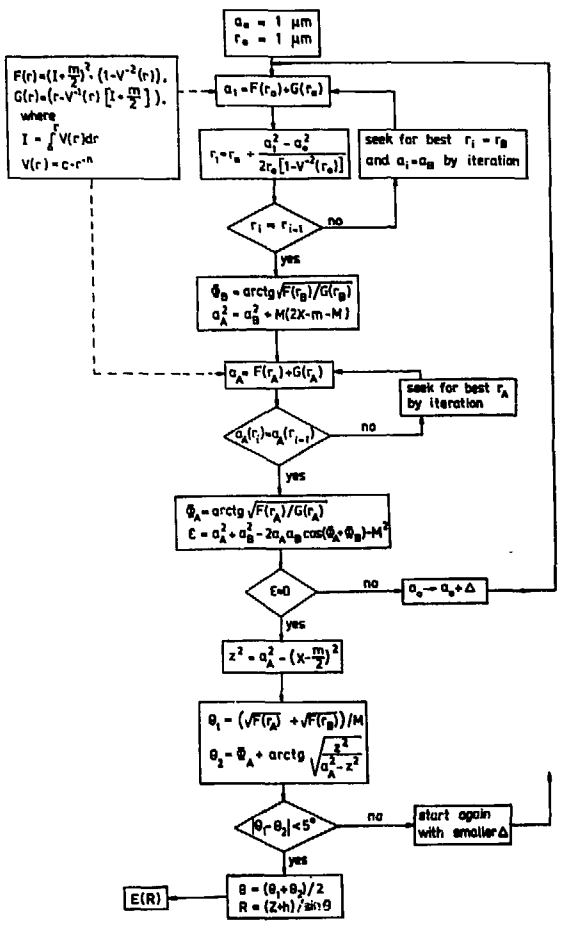

Fig.2. Flow chart to calculate alpha-energy (E) spectrum from track parameters (M,m,X) measured on the surface of CR-39 sheet (see also Fig.4c).

For analysing α-activity distributions in environmental samples we have developed an analogous spectroscopical method employing properly selected, well-measurable etch-track parameters as shown in Fig.4c. The range analysis in our method requires the measurement of three projected track parameters lying in horizontal position on the etched surface of CR-39 detector: major track axis (M), overall projected track length (X) and the diameter of etched-out track end (m). The layer thickness (h) removed from the detector surface during etching should also be known. We note that the latter quantity can be measured also from "horizontal track parameters", namely, from the half minor axis of fission tracks.

In addition to the above-mentioned well-measurable quantities, one has to know the so-called response curve of the track detector itself. For α-particle tracks in CR-39 a power law approximation of the form $V(r) = V_T(r)/V_B = c\cdot r^{-n}$ proves to be applicable, where r is the residual range measured in μm from a general point to the end of particle trajectory, and c and n are fitted constants. We note that c = 11.6 and n = 0.464 for the most sensitive Hungarian CR-39 products (MA-ND/p made by MOM) and c = 5 and n = 0.3 for Homalite (1600 μm) CR-39 if the etchant is 20 % NaOH at 70°C.

Without discussing the origin of various relationships used, in Fig.2 we present a flow chart of our energy calculation programme. It should be noted that if m is equal to zero the calculation scheme provides the etched track length (L) and not the range of particles (R>L).

RESULTS AND DISCUSSION

By using the previous methods, we have analysed several ground-level air samples collected 1) in the garden of Central Institute of Atmospheric Physics nearby Budapest (Oct. 1980 and Jan. 1982), and 2) at different traffic junctions in Debrecen (May-June, 1979 and Jan-Feb 1980). At the first sampling site we have used both Nuclepore filter shown in Fig.4a and glass-fiber filter. In the latter case the aerosols were separated according to their size by a six-stage cascade impactor. At the second site only glass-fiber filter was used.

Our results obtained for filtered air samples (see in Table 1) are in good agreement with other published data determined under comparable geophysical conditions for the middle latitudes of the northern hemisphere (Winkler et al., 1981 and Refs. in their paper). We note that activity concentrations of 14fCi·m^{-3} (0.518 mBq·m^{-3}) for ^{210}Pb and 3.3 fCi·m^{-3} (0.122 mBq·m^{-3}) for ^{210}Po are generally accepted today as global average values (UN. Report, 1977).

TABLE 1 Long-lived radon daughters in surface air, measured by autoradiographs in CR-39

Aerosols filtered (1980 Oct., Budapest)			Aerosols aerodynamically separated (1982 Jan., Budapest)			
Sample No. (Nuclepore filter)	^{210}Pb [mBq·m^{-3}]	^{210}Po [mBq·m^{-3}]	Stage No (Cascade impactor)	Size interval [μm]	^{210}Pb [mBq·m^{-3}]	^{210}Po [mBq·m^{-3}]
1	0.44±0.04	0.04±0.08	1	> 7.2	0.02±0.03	0.04±0.05
2	0.94±0.05	0.0 ±0.10	2	3.0 -7.2	0.06±0.01	0.05±0.01
3	0.65±0.04	0.07±0.10	3	1.5 -3.0	0.11±0.03	0.03±0.04
4	0.23±0.02	0.08±0.05	4	0.96-1.5	0.28±0.06	0.03±0.08
5	0.27±0.03	0.0 ±0.06	5	0.5 -0.96	0.25±0.01	0.12±0.01
			6	<0.5	0.45±0.04	0.31±0.05
Mean:	0.51±0.03	0.04±0.07		Sum:	1.17±0.08	0.58±0.12

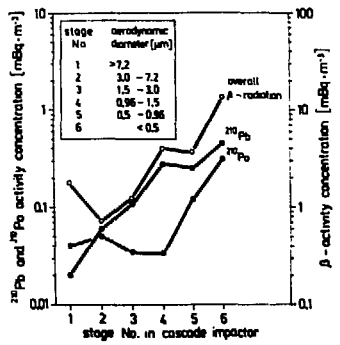

Fig.3 Variation of activity concentration of ^{210}Pb and ^{210}Po with decreasing size of aerosol particles. For comparison, the overall beta-activity, 24 hours after sampling, is also indicated.

In Table 1 activity data measured for size-separated aerosols are also presented. Curves showing the distribution of activity concentration in various size intervals is plotted in Fig.3. The activity concentration of long-lived radionuclides displays the same incresing tendency with decreasing particulate sizes as the overall beta-activity does. This behaviour is in agreement with data reported by other authors. A comprehensive study of the size distribution and possible origin of long-lived radon daughters in the troposhere is published by Moore et al (1978). It has been pointed out that the distribution of long-lived radon daughters in different size intervals of particulates reflects the original attachment distribution. In addition to the originally attached nuclides, the long-lived radioactivity can result from soil resuspension, combustion products and other pollutants. The size distribution and also the A_o(Po)/A_o(Pb) ratio in aerosols are influenced by the latter additional processes.

Our A_o(Po) data derived from track measurements in the small-size fractions differ considerably from those obtained for filtered air samples, where no size separation is made. The higher values of A_o(Po) obtained in the smaller size fractions (see Table 1) may be due to the presence of high amount of aerosols of soil and combustion origin during sampling. This assumption is supported by the high mass concentration observed in the air sample studied.

In case of air samples filtered at different traffic junctions in Debrecen, only A_o(Pb) values are measured. We have got an average of 22.2fC·m^{-3}(0.821 mBq·m^{-3}) for summer period in 1979 and 12.4 fCi·m^{-3}(0.459 mBq·m^{-3}) for winter in 1980. This may reflect the known seasonal variation of the radon content of air above the ground level. We have found only a weak correlation between the long-lived radon daughter content and the dust concentration of air, although a considerable increase of the "normal" lead content in the samples collected during peak traffic time is proved by X-ray analysis.

Finally, we have applied our previously presented programme to the alpha-tracks observed in CR-39 autoradiographs. By using this, we could derive the energy spectrum charachteristic of the alpha-activity of air samples. From the spectrum measured (see Fig.4d) it is apparent that the energy loss in the samples itself is negligible, and the mean energy of alpha-particles is 5.3 MeV as expected for ^{210}Po. The overall energy resolution obtained is ±0.1 MeV.

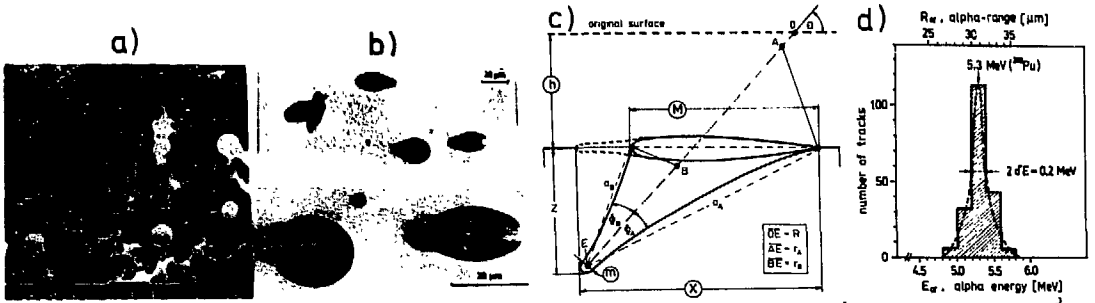

Fig. 4. a) SEM microphotograph of aerosols deposited on Nuclepore when 0.8m^3·cm^{-2} air volume is filtered, b) alpha-tracks in CR-39 after several week exposure in contact with the aerosol-containing filter, c) schematical figure showing track parameters (M,m,X) to be measured for range (R) determination. Other quantities used in the computer programme, shown in Fig.2, are also indicated, d) energy spectrum derived from the parameters of individual alpha-tracks by using the programme presented in Fig.2.

ACKNOWLEDGEMENT

The authors thank K. Bónis and J. Bacsó for providing the samples and related data for the measurements.

REFERENCES

Fews, A. P., and D. L. Hensaw (1982). High resolution α-particle spectroscopy using CR-39 plastic track detector. Proc. 11th Int. Conf. Solid State Nuclear Track Detectors, Bristol, Pergamon Press, 641-645.

Henshaw, D. L., and A. P. Fews (1982). The microdistribution of α-active nuclei in the human lung, II. Results. Proc. 11th Int. Conf. Solid State Nuclear Track Detectors, Bristol, Pergamon Press, 711-715.

Moore, H. E., S. E. Poet, and E. A. Martell (1978). Size distribution and origin of lead-210, bismuth-210, and polonium-210 on airborne particles in the troposphere. Natural Radiation Environment III. Vol. I. Houston, pp. 415-429.

UN Scientific Committee on the Effects of Atomic Radiation (1977). Sources and effects of ionizing radiation. Report to the General Assembly, New York, p. 62.

Winkler, R., H. Hötzl, and B. Chatterjee (1981). Analysis of ^{210}Pb and ^{210}Po concentrations in surface air by an α-spectrometric method. Health Phys., 41, 495-503.

ATOMKI Preprint E/12 (1983)

MEASUREMENT OF RADON, RADON DAUGHTERS AND THORON CONCENTRATIONS BY MULTI-DETECTOR DEVICES

G. Somogyi*, B. Paripás** and Zs. Varga*

*Institute of Nuclear Research of the Hungarian Academy of Sciences, H-4001 Debrecen, Hungary
**Institute for Public Health and Epidemics, H-3501, Miskolc, Hungary

ABSTRACT

There is a growing interest in collection of data concerning human exposures to naturally occurring alpha-emitting radionuclides (e.g. in mines, dwellings, building materials, industrial wastes, coal fuel cycle, water supply, soil, plants, etc). Most of such studies is incomplete for the following reasons: 1) In radon measurements the contribution of thoron is generally neglected, 2) The determination of equilibrium factor is complicated or not possible at all. 3) Short- and long-term concentration fluctuations cause difficulties in obtaining representative mean values. 4) The plate-out effect is generally not taken into account. We have studied a variety of simple methods that could be used to overcome some of these difficulties by using cups equipped with two or more alpha-sensitive nuclear track detectors. A theoretical foundation of the quantitative measurements with such devices is presented. Experimental data are reported on radon, radon daughters and thoron concentrations measured by multi-detector devices in cave soil gas and in air of Hungarian dwellings.

KEYWORDS

Radon, thoron; alpha-activity measurements; radioactive equilibrium; LR-115 and CR-39 track detectors; multi-detector devices; dwelling, soil gas.

INTRODUCTION

The health hazard for the population in the environment results mostly from the alpha-radioactive nuclides (radon, thoron and their decay products) being present in the air of living houses and various working places. For a real estimation of the average population exposure the most reliable method is the use of alpha-sensitive plastic track detectors (e.g. LR-115 and CR-39) for integrating, long-term measurements. Although the superiority of this passive measuring method has been clearly demonstrated by several works, some problems still need to be solved. The purpose of our paper to propose certain methodical and/or evaluation improvements to overcome or reduce these problems.

One of the principle tasks is related to the understanding of the response of bare plastic track detectors placed into a can-type measuring device. The response is obviously determined by the can geometry and the position and registration sensitivity of the detector. By changing these parameters and/or using more than one detector at different positions one may expect improvements and more information for the estimation of radiation exposure due to various alpha-active nuclides. In this way one may gain simultaneous information on the radon exposure (E_{Rn}), total alpha-exposure (E_t), thoron and its daugters exposure (E_{T_nD}) equilibrium factor (F), and even separately on the concentration of alpha-active decay products (polonium isotopes).

RESPONSE IN A CYLINDRICAL DEVICE

Quantitative measurements with both single and multi-detector devices can

be performed only if the response of detectors (observed tracks per unit radon or daughter concentration) is known. It can be estimated experimentally or theoretically. For constructing special measuring devices, the theoretically derived response relations may supply reasonable basic design criteria. Mathematical base for such calculations is reported by Fleischer and Mogro-Campero (1978) and the response is demonstrated for few devices of specific geometry. By the extention of these calculations, we have derived a complete set of relations for describing the response of LR-115 and CR-39 track detectors at the top of a cylindrical device as a function of its radius (a) and length (h).

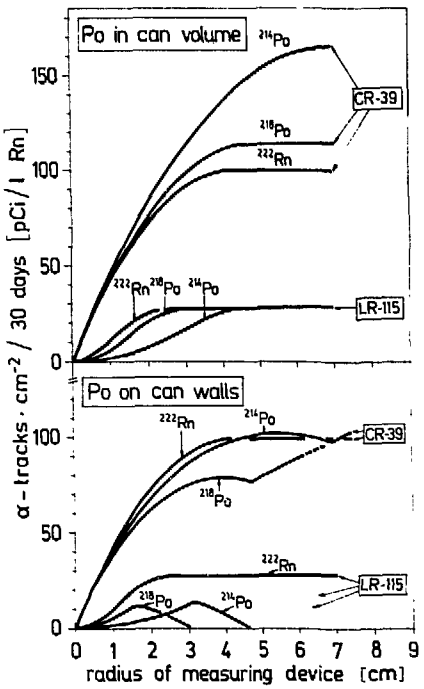

Fig.1. Response of LR-115 and CR-39 to radon and its daughters, calculated by the relations in Table 1 for equilibrium condition, assuming that the Po isotopes are a) deposited completely on the internal can walls (including the detector also) and b) distributed only in the can volume.

TABLE 1 Relations for calculating the track density observable in LR-115 and CR-39 detectors at the top of a can-type device of a radius and h length.

POSITION OF α-ACTIVITY	VALIDITY OF RELATIONS ($a_1=R_1\cos\theta_{c1}$; $a_0=R_0\cos\theta_c$)	BASIC RELATIONS ($\theta_0=\arccos(a/R_0)$; $\theta_1=\arccos(a/R_1)$; $\theta_R=\arccos(a/R)$,)	FINAL RELATIONS (R_0<R_{min}; R_1<R_{max}; R=α-ranges in air; c=96tracks·cm^{-2}/30days for 1pCi/ℓ radon)
DETECTORS FOR LR-115: CAN VOLUME (V=$a^2\pi h$)	$0\le a\le a_1$	$\frac{c}{4\pi}\int_{R_1}^{R_0}\int_0^{\pi/2}\sin2\theta d\theta dR$	$\frac{c}{4\pi}a(\frac{a}{R_1}-\frac{a}{R_0})$
	$a_1\le a\le a_0$	$\frac{c}{4\pi}\int_{R_1}^{a/\cos\theta_c}\int_{\theta_c}^{\pi/2}\sin2\theta d\theta dR+\frac{c}{4\pi}\int_{a/\cos\theta_c}^{R_0}\int_{\theta_R}^{\pi/2}\sin2\theta d\theta dR$	$\frac{c}{4\pi}a\cos\theta_c(2-\frac{a_1}{a}-\frac{a}{R_0})$
	$a_0\le a$	$\frac{c}{4\pi}\int_{R_1}^{R_2}\int_{\theta_c}^{\pi/2}\sin2\theta d\theta dR$	$\frac{c}{4\pi}(R_{max}-R_{min})\cos^2\theta_c$
DETECTORS FOR LR-115: "TOTAL" CAN SURFACE ($S=2a^2\pi+2a\pi h$)	$0\le a\le a_1$	$\frac{c}{2}\frac{V}{S}\int_{\theta_1}^{\theta_0}\sin\theta d\theta$	$\frac{c}{4\pi}\frac{h}{a\pi h}(\frac{a}{R_1}-\frac{a}{R_0})$
	$a_1\le a\le a_0$	$\frac{c}{2}\frac{V}{S}\int_{\theta_c}^{\theta_0}\sin\theta d\theta$	$\frac{c}{4\pi}\frac{h}{a\pi h}(\cos\theta_c-\frac{a}{R_0})$
	$a_0\le a$	0	0
DETECTORS FOR CR-39: CAN VOLUME (V)	$0\le a\le R$	$\frac{c}{4\pi}\int_0^{a}\int_0^{\pi/2}\sin2\theta d\theta dR+\frac{c}{4\pi}\int_a^{R}\int_{\theta_R}^{\pi/2}\sin2\theta d\theta dR$	$\frac{c}{4\pi}a(2-\frac{a}{R})$
	$R\le a$	$\frac{c}{4\pi}\int_0^{R}\int_0^{\pi/2}\sin2\theta d\theta dR$	$\frac{c}{4\pi}R$
DETECTORS FOR CR-39: "TOTAL" CAN SURFACE (S)	$0\le a\le R$	$\frac{c}{2}\frac{V}{S}(\int_0^{\pi/2}\sin\theta d\theta+\int_{\theta_R}^{\pi/2}\sin\theta d\theta)$	$\frac{c}{4\pi}\frac{h}{a\pi h}(2-\frac{a}{R})$
	$R\le a$	$\frac{c}{2}\frac{V}{S}\int_0^{\pi/2}\sin\theta d\theta$ (plate-out)	$\frac{c}{4\pi}\frac{h}{a\pi h}$

*For LR-115(13 μm) $\theta_c\approx40^\circ$, $R_{min}\approx0.8$μm, $R_{max}\approx2.77$μm at 5 μm residual thickness.
**For CR-39 we assumed that $\cos\theta_c\approx1$ and sensitive for plate-out effect.

In Table 1 relations for two possible limit cases are given: i) when the alpha-active nuclides are completely and uniformly deposited on the can walls (including the detector also), and ii) when they are distributed in the can volume. For not too large can volumes the case i) is well satisfied for daughter nuclei (Po-218, Po-214), as they have high probability of plating out on the can walls before decaying. The case ii) is perfectly applicable to the radon gas (Rn-222). The thoron (Rn-220), due to its short half-life, is generally not uniformly distributed in an open can.

The calculated response of LR-115 and CR-39 detectors to the alphas of Rn Po-218 and Po-214 nuclei is presented in Fig.1. For polonium nuclei the response is given in tracks·cm^{-2} per 30 days for radioactive equilibrium with 1 pCi/ℓ radon. In the calculation it is assumed that for LR-115 $\theta_c\approx40^\circ$, while for CR-39 $\theta_c\approx0^\circ$. From Fig.1 it is obvious that for the usual can geometry (3-4 cm radius) the CR-39 is very sensitive for the presence of daughters but the LR-115 is practically not. It is also interesting to note that in a narrow tube of about 1-1.5 cm radius the CR-39 response becomes independent on the actual position (can wall or volume) of daughter nuclei. In this case a measuring uncertainty due to the unknown percentage of attachment to airborne aerosol particulates can be completely excluded. At the same time, the response is identical for all the alpha-active nuclei considered.

CONSTRUCTION OF SINGLE AND MULTI-DETECTOR DEVICES

Optimum construction of single and multi-detector measuring devices depends on the particular field of application. In Fig.2 we summarized some useful configurations. In practice, from among the the single-detector devices, we have prefered the device 1c for radon measurements in air and the device 1d for under-water measurements. The device 1c is a simple "thermostated can" having double-wall filled up with water. With this we could avoid, even in the most severe weather conditions, the known problem due to the water condensation on the detector surface (Likes et al, 1979; Abu-Jarad and Fremlin, 1982).

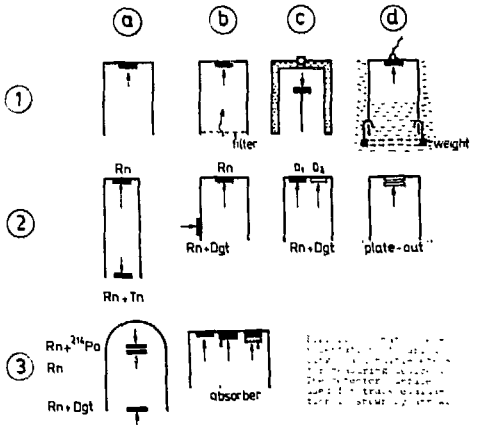

For monitoring thoron and its daughters we have developed a "long-tube" construction (device 2a) equipped with two LR-115 detectors. We have been using this design in our routine radon surveying in the ground since 1978 and our experiences have shown that in a 30 cm long tube the upper detector can easily measure the radon signal even in a 100 times higher thoron background (see Fig. 3.). Combining the main elements of the devices 1c and 2a, one can also avoid the development of a disturbing air convention in the tube.

The device 2b was first applied by Frank and Benton (1977) for simultaneous estimation of radon and equilibrium factor. Such a device was also successfully applied by us to large-scale radon monitoring in Hungarian houses (Fig.4). We have found that by a filter-covered version of this device, one can estimate even the alpha-activity contribution resulting from thoron and its daughters (see Fig.5). The device 2c has been used by us for monitoring the degree of radioactive equilibrium (its principle see in Fig. 6). Here two internal detectors of different sensitivity (LR-115 and CR-39) should be used.

The device 2d equipped with two CR-39 detectors in a few millimeter distance from each other may be proposed to monitor the degree of plate-out effect. In the small gap between the detectors the radon signal is negligible, but the detectors show doubled plate-out reading because the internal surfaces can register the alphas of daughter nuclei plating out on both the own and opposite surfaces. Finally, we consider the three-detector devices. The device 3b in Fig.2 is designed by us with three LR-115 detectors. Its working principle is shown in Fig.7. The first basic requirement of a correct measurements of the individual radon and daughter concentrations with such a device is a reasonably complete and homogeneous plate-out of the polonium nuclei on the internal walls. This can be well satisfied with the use of a properly designed metalic can. The second

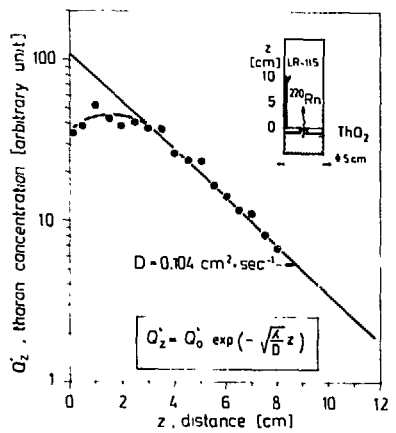

Fig.3. Steady-state concentration distribution of thoron along the height of a closed cylindrical can.

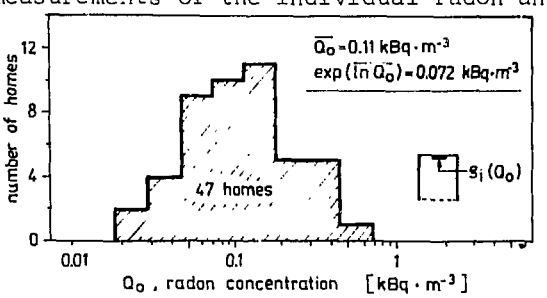

Fig.4. Frequency distribution of the activity concentration of radon in 47 houses, measured with internal LR-115 films (1980 Dec.- 1981 May).

requirement is the chose of a particular radius for the sphere portion covering the cylindrical tube. Preliminary experiences with our first three-detector devices (r=5.1 cm, a=4 cm) have indicated that such a design could give resonable results (see Fig.8) if the measurement conditions are not very extreme (e.g. high thoron or aerosol content). An active device for separate radon and daughters monitoring, similar to the device 3b, with detectors covered by absorbers of proper thickness, has been using in routine work by Chapuis et al (1972). It may be worth trying to develop an analogous design as passive dosemeter as well.

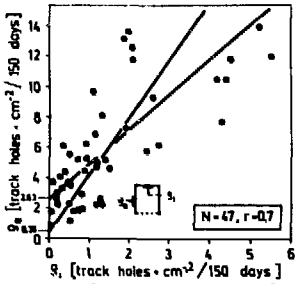

Fig.5. Correlation between the readings of external (ϱ_e) and internal (ϱ_i) LR-115 films in 47 houses. Solid lines are regression curves for the two variables.

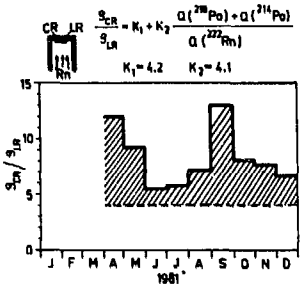

Fig.6. Seasonal variation of the ratio of the readings of internal CR-39 and LR-115 detectors in cave air.

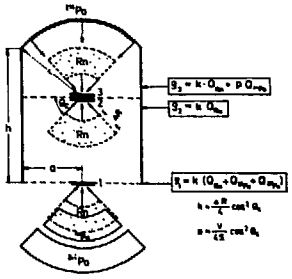

Fig.7. Schematic representation of a three-detector device designed by us (V=can volume, S=internal surface, ΔR=1.9cm, θ_c=40° for LR-115(13μm) etched to 5 μm residual thickness).

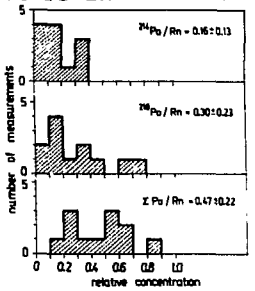

Fig.8. Polonium/radon concentration ratios in cave air determined with the device shown in Fig.7 (1982 April-1983 March).

SOME QUANTITATIVE ASPECTS OF THE MEASUREMENTS

Finally, we present here some useful quantitative relations and additional remarks to our experiments.

i) Radon exposition (E_{Rn}). The radon exposition is given by an integral of the radon activity concentration (Q_o) during the exposure time, T, :

$$E_{Rn} = \int_o^T Q_o(t)dt \ . \qquad (1)$$

If we use the device 1b which excludes the thoron and its daughters (Fleischer et al, 1980), the penetrability of radon through the filter should be taken into account. The radon activities in (Q_{oi}) and outside (Q_o) the can will not be identical but determined by the following equation (Fleischer et al, 1980):

$$dQ_{oi}/dt = (DA/\delta V)(Q_o - Q_{oi}) - \lambda Q_{oi} \ , \qquad (2)$$

where D is the diffusion coefficient of radon in the filter, λ is radon decay constant, V is the can volume and A and δ are the area and thickness of the filter. If after integration we introduce the registration efficiency of the detector, η, and the filtering coefficient $k_f^{-1}=1+(V\lambda\delta/DA)$, we have:

$$\rho_i/\eta = \int_o^T Q_{oi}dt = k_f E_{Rn} + \lambda^{-1}(1-k_f)[Q_{oi}(0)-Q_{oi}(T)]. \qquad (3)$$

From here we can see that the proportionality condition

$$E_{Rn} = k_f^{-1} \cdot \eta^{-1} \cdot \rho_i \qquad (4)$$

between E_{Rn} and the internal track density, ρ_i, can be fulfilled only if $Q_{oi}(0)=Q_{oi}(T)$. This can be well satisfied if we cover the measuring can by the filter in radon-free atmosphere and, after completing the measurement, we wait a few days again in the same atmosphere before opening the can.

ii) Total alpha-expositon (E_t). The total alpha-exposition, which can be monitored by the track density ρ_e measured on an external detector, is defined by

$$E_t=\eta^{-1}\rho_e=\int_0^T(Q_o+Q_1+Q_3+Q_o'+Q_1'+2Q_3')dt, \qquad (5)$$

where Q_o, Q_1, Q_3, Q_o', Q_1', Q_3' refer to the ^{222}Rn, ^{218}Po, ^{214}Po, ^{220}Rn, ^{216}Po and $^{212}Bi(^{212}Po)$ activiti concentrations, respectively. We note that the $E_t=\eta^{-1}.\rho_e$ relation is valid only for LR-115 detector in "thick air" where the registration efficiency, η, is independent on the alpha-energy, as it can be seen from the respective relation given in Table 1 (if $a_o \leq a$).

iii) Thoron and its daughters exposition (E_{TnD}). As we have pointed out (see Fig.3) the thoron concentration in a closed long tube without no convention, shows an exponential decrease with the tube height. This behaviour can be used for separate measurement of the thoron and radon. We have found another possibility to estimate the mean exposure due to thoron and its daughters. To this, we have to measure a given number of ρ_e and ρ_i data with a filter-covered version of device 2b and then to plot the regression lines for both variables (see Fig.5). These lines will intersect the origin in absence of thoron but lift up if thoron is "seen" by the external detector. The curve of the most probable stochastic correlation between ρ_e and ρ_i should ran between the two regression lines. In Fig.5 it is represented by the equation $\rho_e=1.6+2.9\ \rho_i$. From here, the mean track density due to thoron and its daughter (ρ_{TnD}) in these 47 homes is 1.6 track holes.mm^{-2}/150 days, which is comparable with the effect of radon exposure (2.1 track holes mm^{-2}/150 days equivalent with 0.11 kBqm^{-3} as shown in Fig.4).

iv) Equilibrium factor (F). The mean equilibrium factor ($\bar{F}$) is determined by the relation $\bar{F}=(0.1\bar{Q}_1+0.52\bar{Q}_2+0.38\bar{Q}_3)/\bar{Q}_o$.($\bar{Q}_2$ is the mean activity concentration of ^{214}Pb, the others are the same as mentioned under section ii)). $\bar{F}$ exactly cannot be determined from two-detector measurements, but a reasonable estimation can be obtained from the measurable quantity $k_f(\rho_e-\rho_{TnD})/\rho_i=(\bar{Q}_o+\bar{Q}_1+\bar{Q}_3)/\bar{Q}_o$ by using the fact that the correlation between the latter ratio and $\bar{F}$ is restricted to a relatively narrow region. Taking into account typical aerosol and ventilation parameters, and the $(\rho_e-\rho_{TnD})/\rho_i=2.9$ value from Fig.5, from the Jacobi (1972) equations we got the value $\bar{F}=0.4$ for 47 homes.

REFERENCES

Abu-Jarad, F., J. H. Fremlin (1982). Radon emanation from uranium corridor in Orkney island and Kinver caves. Proc. 11th Int. Conf. Solid State Nuclear Track Detectors, Bristol, Pergamon Press. 565-568.

Chapuis, A. M., D. Dajlevic, Ph. Duport, and G. Soudain (1972). Dosimetrie du radon. Proc. 8th Int. Conf. Nucl. Photog. and SSNTD, Bucharest, Vol.II. 319-328.

Fleischer, R. L., and A. Mogro-Campero (1978). Mapping of integrated radon emanation for detection of long-distance migration of gases within earth: techniques and principles. J. Geophys. Res., 83, 3539-3549.

Fleischer, R. L., W. R. Giard, A. Mogro-Campero, L. G. Turner, H. W. Alter, and J. E. Gingrich (1980). Dosimetry of environmental radon: methods and theory for low-dose, integrated measurements. Health Phys., 39, 957-962.

Frank, A. L., and E. V. Benton (1977). Radon dosimetry using plastic nuclear track detectors. Nucl. Track Detection, 1, 149-179.

Jacobi, W. (1972). Activity and potential α-energy of radon and radon-daughters in different air atmospheres. Health Phys., 22, 441-450.

Likes, R. S., A. Mogro-Campero, and R. L. Fleischer (1979). Moisture-insensitive monitoring of radon. Nucl. Instrum. Meth., 159, 395-400.

HU 8508613

ATOMKI Preprint E/13 (1983)

MEASUREMENT OF THE $^{12}C(^{12}C,^{8}Be_{g.s.})^{16}O_{g.s.}$ CROSS SECTION AT SUBBARRIER ENERGIES BY PLASTIC DETECTORS

I. Hunyadi*, I.M. Szöghy and B. Čujec

Université Laval, Québec, Canada G1K 7P4
*Visiting scientist from Institute of Nuclear Research of the Hungarian Academy of Sciences, H-4001 Debrecen, Hungary

ABSTRACT

The astrophysically significant yields for the $^{12}C(^{12}C,^{8}Be_{g.s.})^{16}O_{g.s.}$ reaction have been measured at several incident energies between $2.4 < E_{c.m.}(MeV) < 6.4$, detecting α-particles from the $^{8}Be_{g.s.} \rightarrow 2\alpha$ decay in the forward directions by a Mylar shielded Makrofol-E type polycarbonate foil. The α_0 and α_1 groups from the $^{20}Ne+\alpha$ channels were separately counted at backward angles in the same foil. Compared to the α_0 and α_1 groups the yield for the $^{12}C(^{12}C,^{8}Be)^{16}O$ reaction becomes increasingly more important with decreasing energy. The measured angular distributions are indicative of an α-transfer.

KEYWORDS

$^{12}C+^{12}C$ system, heavy-ion reactions, subbarrier cross sections, α-transfer reactions, reaction mechanisms, plastic track detectors.

EXPERIMENT AND RESULTS

The $^{12}C(^{12}C,^{8}Be_{g.s.})^{16}O_{g.s.}$ reaction has been studied previously over the incident energy interval of $9 < E_{c.m.}(MeV) < 20$ by the coincident detection of α-particles from the $^{8}Be \rightarrow 2\alpha$ decay (Fletcher and co-workers, 1976), and the energy interval $6 < E_{c.m.}(MeV) < 11$ by the ΔE-E telescope detection of ^{16}O particles (Wada and co-workers, 1980). Though the knowledge of cross section for this reaction is of decisive importance for the evaluation of the $^{12}C+^{12}C$ total reaction cross section as well as for the understanding of the $^{12}C+^{12}C$ resonance and interaction mechanisms, no measurements were yet performed at subbarrier energies ($E_{c.m.} < 6$ MeV). At low energies the detection by electronic devices is difficult because of the negative reaction Q-value (-0.282 MeV), resulting in low energy of α-particles from $^{8}Be \rightarrow 2\alpha$ and low energy recoiling ^{16}O, and because of a huge background of ^{12}C and protons, arising from the elastic scattering of the ^{12}C beam on the carbon target and its hydrogen contaminants. Certain plastic foils due to their insensitivity to protons, are ideal in such circumstances.

We report here on the measurement of the $^{12}C(^{12}C,^{8}Be)^{16}O$ yields performed, at several incident energies between $2.4 < E_{c.m.}$ (MeV) < 6.4, by the detection of α-particles (from $^{8}Be \rightarrow 2\alpha$) with 200 μm thick Makrofol E polycarbonate foils, sensitive to α-particles and heavier ions. The yields for the α_0,α_1, and $\alpha_{4,5}$ groups from the $^{20}Ne+\alpha$ channel (see Fig. 1) were measured simultaneously for comparison with previous measurements (Becker and co-workers, 1981) and for normalization purposes.

The experimental arrangement is shown in Fig. 2. A 13 mm wide Makrofol strip, forming a cylinder of 4 cm radius with holes, 6 mm in diameter, punched at 0°, 170° and 180° with respect to the beam direction, was exposed at each incident energy. In order to reduce the background due to the scattered beam, a cylindric mask was positioned between the target and detector. The $^{8}Be \rightarrow 2\alpha$ and $\alpha_{4,5}$ groups were detected in the forward part of the strip, shielded by Mylar absorbers of varying thickness chosen to stop the elastically scattered ^{12}C-particles. The α_0 and α_1 groups were detected in the backward part of the strip which was shielded by aluminum absorbers of varying thickness chosen such as to stop the α_2 group (see Fig. 3). The $^{12}C^{+}$ and $^{12}C^{++}$ beams of 0.1 to 1 μA current were used in conjuction with 10 and 30 μg/cm^2 natural carbon targets. The exposure time varied between a fraction of an

hour and two days (at the lowest energy) to obtain a convenient track density, ideally 50 to 400 tracks/mm^2. It was estimated beforehand from short test runs, used to check absorbers.

The etching of Makrofol-detectors was performed at the controled temperature of (70.0±0.1) °C in the PEW solution of 30 g KOH + 90 mℓ H_2O + 100 mℓ C_2H_5OH, recommanded by Somogyi and co-workers (1977), with an etching rate of about 20 μm per hour. The action of solution was periodically checked by detector samples irradiated with α-particles from an ^{241}Am source. It is interesting to note that during the $E_{c.m.}$ = 2.93 MeV exposure the detector strip was not covered by absorbers near the detection angles θ_L=15° and θ_L=25° giving rise to a large ^{12}C background. This background was, however, succesfully removed by etching and the ^{8}Be→2α group appeared quite clearly (Fig. 4).

The possibility of contribution from light contaminants in the target was examined by irradiating self supporting targets of Li, Be and B with the ^{12}C beam at a few energies. It was concluded that reactions with these contaminants do not contribute to the ^{8}Be→2α group studied.

Figure 5 shows the angular distributions obtained in this measurement for the ^{8}Be→2α, α_0, α_1 and $\alpha_{4,5}$ groups at various incident energies. The angular distributions for the ^{20}Ne+α channels are presented in the center-of-mass system and are symmetrical around 90°. The angular distributions for the two α-particles from the ^{16}O+^{8}Be channel (extreme left in Fig. 5) are presented in the laboratory system, the transformation of the data to the center-of-mass ^{8}Be-angle being still in progress using Monte Carlo type simulations (Karp and co-workers, 1983). Note that the α-yields from the ^{16}O+^{8}Be channel become, with decreasing incident energy, increasingly more forward peaked and higher with respect to the α-yields from the ^{20}Ne+α channels. This is indicative of an α-transfer mechanism in the ^{12}C(^{12}C,^{8}Be)^{16}O reaction at energies substantially below the interaction barrier. A quantitative interpretation of data is in progress.

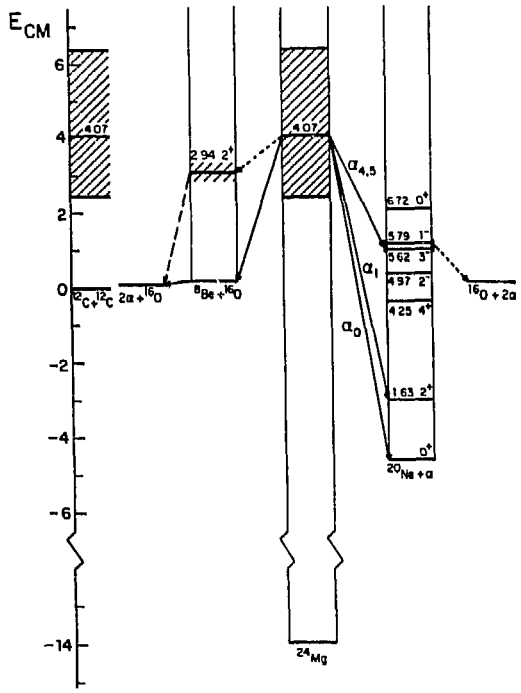

Fig. 1. Energy level diagram for the α-particle channels of the ^{12}C+^{12}C reaction. The energy region and the α-groups investigated in the present work are indicated by cross-hatching and solid arrows, respectively.

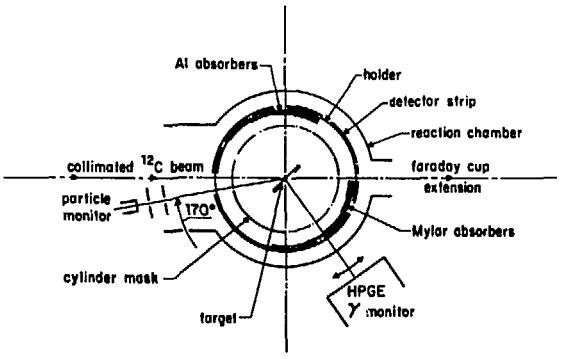

Fig. 2. A shematic view of the reaction chamber used for the exposure of the Makrofol detectors to the α-particles from the ^{12}C+^{12}C reaction.

Fig. 3. Experimental conditions for the exposure at $E_{lab} \approx 10$ MeV ($E_{c.m.} = 4.99$ MeV) beam energy, showing (a) the energy of the elastically scattered ^{12}C and of the α-particles from the $^{20}Ne \rightarrow \alpha$ and $^{16}O + {}^{8}Be$, $^{8}Be \rightarrow 2\alpha$, channels, (b) the thickness of the absorber placed before the plastic detector at various detection angles, and (c) the expected range of the various α-particle groups in the Makrofol-E plastic detector, as functions of the detection angle.

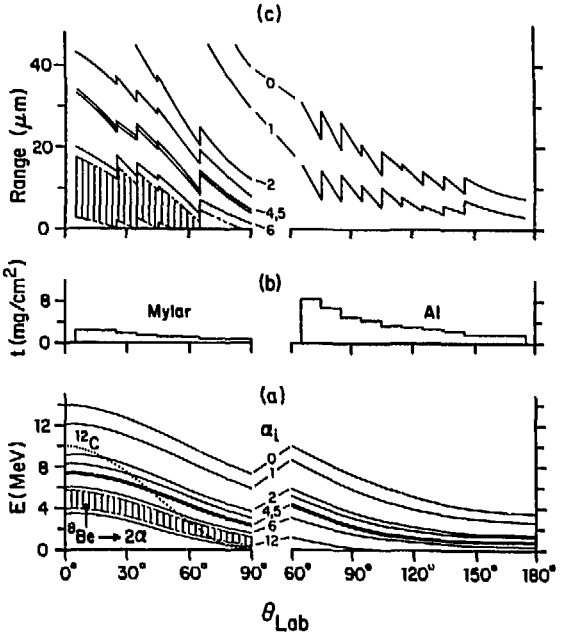

Fig. 4. The diameter distribution and colour of α-tracks in the region of the $^{8}Be \rightarrow 2\alpha$ group. The top histograms are for the exposure at beam energy $E_{c.m.} = 2.93$ MeV, obtained after removal (by etching) of a surface-layer thickness h=6μm. The bottom histograms are for $E_{c.m.} = 2.43$ MeV and h=5μm. The elastically scattered ^{12}C-particles penetrated the Makrofol detectors in the $E_{c.m.} = 2.93$ MeV exposure at detection angles θ_L=15° and 25°, due to uncomplete shielding by the absorbers at these positions.

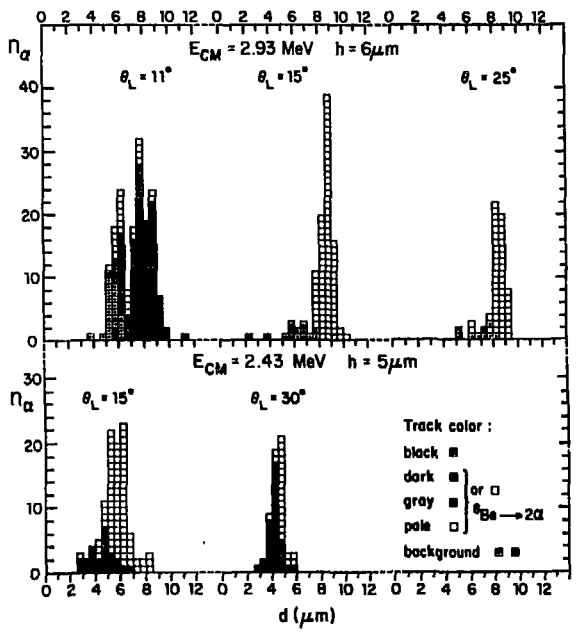

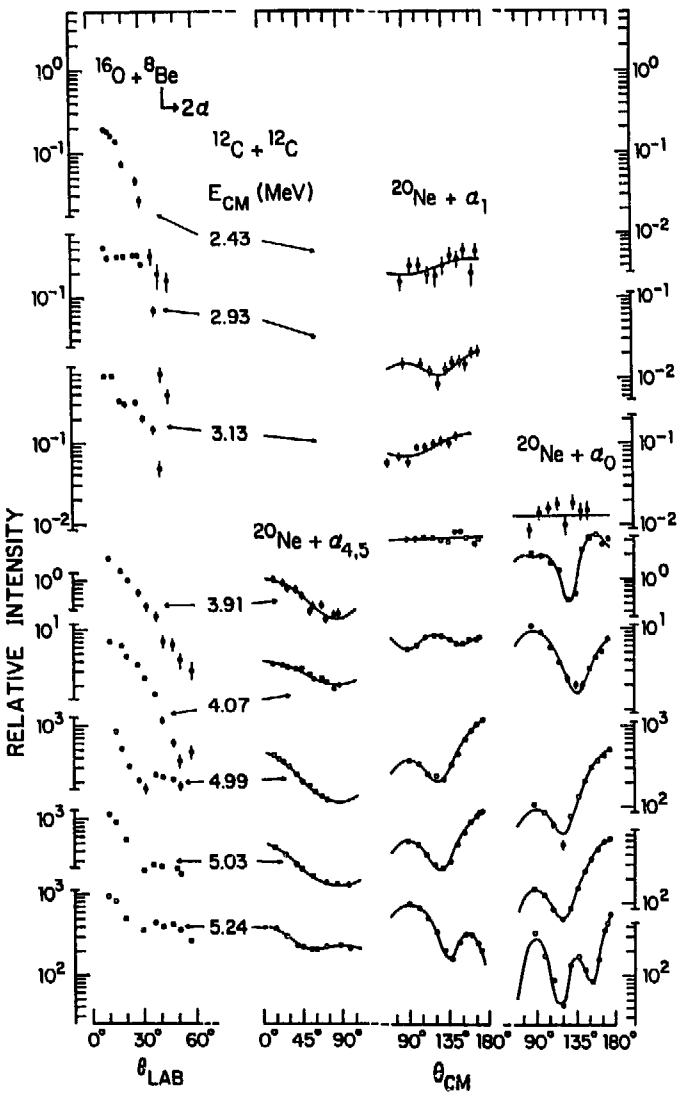

Fig. 5 Angular distributions for the observed α-particle groups. The angular distributions for the $^{20}Ne+\alpha$ channels are in the center-of-mass system, while for the $^{16}O+{}^{8}Be$, $^{8}Be\rightarrow 2\alpha$ channel are in the laboratory system. The statistical errors are indicated when they exceed the point size.

REFERENCES

Becker, H.W., K.U. Kettner, C. Rolfs, and H.P. Trautvetter (1981). Z. Phys., A303, 305-312.

Fletcher, N.R., J.D. Fox, G.J. KeKelis, G.R. Morgan, and G.A. Norton (1976). Phys. Rev., C13, 1173-1179.

Karp, J.S., D. Abriola, R.L. McGrath, and W.A. Watson III (1983). Phys. Rev., C27, 2649-2655.

Somogyi, G., I. Hunyadi, E. Koltay, and L. Zolnai (1977). Nucl. Instr. Meth., 147, 287-295.

Wada, R., T. Murakami, E. Takada, M. Fukada, and K. Takimoto (1980). Phys. Rev., C22, 557-564.

Kiadja a
Magyar Tudományos Akadémia
Atommagkutató Intézete

A kiadásért és szerkesztésért felelős:
dr.Berényi Dénes, az intézet igazgatója

Készült az ATOMKI nyomdájában